Advances in Applied Mathematics and Mechanics
Adv. Appl. Math. Mech., Vol. **18**, No. 1, pp. 134-169

DOI: 10.4208/aamm.OA-2023-0317
February 2026

Energy Conservative Local Discontinuous Galerkin Methods for the Euler-Korteweg Equations

Xiangyi Meng[1,2], Yan Xu[1,*] and J. J. W. Van der Vegt[2]

[1] *School of Mathematical Sciences, University of Science and Technology of China, Hefei, Anhui 230026, China*
[2] *Mathematics of Computational Science Group, Department of Applied Mathematics, University of Twente, Enschede, 7500 AE, The Netherlands*

Received 10 December 2023; Accepted (in revised version) 29 June 2024

Abstract. In this paper, we develop through a careful selection of the auxiliary variables and numerical fluxes an energy conservative local discontinuous Galerkin (LDG) method based on a hybrid form of the general Euler-Korteweg (EK) equations with a variable capillarity coefficient. This energy conservative LDG discretization is of optimal order of accuracy for alternating numerical fluxes, but not for central numerical fluxes which result in the reduction of one order of accuracy when odd degree polynomial basis functions are used. Also, a relatively simple energy conservative LDG discretization for the EK-equations with an irrotational velocity field is presented. Due to the presence of a highly nonlinear third-order spatial derivative term, which originates from the divergence of the Korteweg stress tensor, we employ the novel semi-implicit spectral deferred correction (SDC) method as temporal discretization. The SDC method can be applied to highly nonlinear ordinary differential equations (ODEs) without separating stiff and non-stiff components and is numerically stable for a time step proportional to the mesh size. Numerical experiments, including ones with adaptive meshes, are performed to illustrate the accuracy and capability of the proposed methods to solve the EK-equations.

AMS subject classifications: 65M60, 35Q35

Key words: Euler-Korteweg equations, energy conservation, local discontinuous Galerkin methods, spectral deferred correction methods.

1 Introduction

In this work, we concentrate on the design of local discontinuous Galerkin (LDG) methods for the Euler-Korteweg (EK) equations with a variable capillarity coefficient, coupled

*Corresponding author.
Emails: mxy6@mail.ustc.edu.cn (Xiangyi Meng), yxu@ustc.edu.cn (Yan Xu), j.j.w.vandervegt@utwente.nl (J. J. W. Van der Vegt)

 ©2026 Global Science Press

with a novel semi-implicit spectral deferred correction (SDC) time discretization method. These equations take the surface tension of interfaces into consideration using a capillarity coefficient when modeling the dynamics of an isothermal compressible fluid, and read [5]

$$\rho_t+\nabla\cdot(\rho\mathbf{u})=0, \tag{1.1a}$$
$$(\rho\mathbf{u})_t+\nabla\cdot(\rho\mathbf{u}\otimes\mathbf{u}+p\underline{I})=\nabla\cdot\underline{K}, \tag{1.1b}$$

in $\Omega\times(0,T]$, $\Omega\subset\mathbb{R}^d$, $d\leq 3$, $T>0$, where ρ is the density, $\mathbf{u}\in\mathbb{R}^d$ the fluid velocity, $p=p(\rho)$ the pressure, $\underline{I}$ the identity matrix and $\otimes$ the tensor product. The matrix $\underline{K}$ denotes the Korteweg stress tensor and is defined as

$$\underline{K}=\left(\rho\kappa(\rho)\Delta\rho+\frac{1}{2}(\rho\kappa'(\rho)+\kappa(\rho))|\nabla\rho|^2\right)\underline{I}-\kappa(\rho)\nabla\rho\otimes\nabla\rho, \tag{1.2}$$

with $\kappa=\kappa(\rho)$ the capillarity coefficient. The highly nonlinear third order dispersive term $\nabla\cdot\underline{K}$ can be reduced to the simplified form

$$\nabla\cdot\underline{K}=\rho\nabla\left(\kappa(\rho)\Delta\rho+\frac{1}{2}\kappa'(\rho)|\nabla\rho|^2\right).$$

The EK-equations (1.1) then can be written in an equivalent non-conservative form as

$$\rho_t+\nabla\cdot(\rho\mathbf{u})=0, \tag{1.3a}$$
$$\mathbf{u}_t+\mathbf{u}\cdot\nabla\mathbf{u}+\nabla F'(\rho)=\nabla\left(\kappa(\rho)\Delta\rho+\frac{1}{2}\kappa'(\rho)|\nabla\rho|^2\right), \tag{1.3b}$$

with $F=F(\rho)$ the free energy density, which relates to the pressure p through the relation

$$p(\rho)=\rho F'(\rho)-F(\rho).$$

For a capillary fluid, unlike a regular isothermal fluid, the total energy on Ω takes the form

$$\mathcal{H}=\int_\Omega\left(\frac{1}{2}\rho|\mathbf{u}|^2+F(\rho)+\frac{1}{2}\kappa(\rho)|\nabla\rho|^2\right)d\mathbf{x}, \tag{1.4}$$

which shows that regions with large density gradients can contribute significantly to the total energy.

The EK-equations can be endowed with a non-monotone van der Waals equation of state [35]

$$p(\rho)=Rb\frac{\theta\rho}{b-\rho}-a\rho^2, \tag{1.5}$$

with temperature θ, universal gas constant R and positive constants a, b depending on the fluid, which allows the modelling of liquid-vapor mixtures undergoing a phase transition, i.e., there is mass transfer driven by thermodynamics between the phases. As a

mixed hyperbolic-elliptic system, this model belongs to the well-known diffuse-interface models, which treat the interface as a thin layer where physical quantities vary smoothly. It can be traced back to van der Waals [49] and Korteweg [34], and was actually derived in the modern form using the second gradient theory by Dunn and Serrin [20]. Several special cases of the EK-equations have also arisen in other physical fields, e.g., in water wave theory, when the capillarity coefficient κ is chosen to be constant, and in quantum hydrodynamics (QHD), when $\kappa(\rho)$ is proportional to $1/\rho$. In particular, the QHD equations can be used to describe quantum semiconductors [22], quantum trajectories of Bohmian mechanics [50], superfluids [37] and weakly interacting Bose gases [26]. Serious difficulties may, however, be encountered when solving the EK-equations. For example, the treatment of the third-order highly nonlinear term and the possible mixed hyperbolic-elliptic character of the equations are non-trivial. Besides, compared with the Navier-Stokes-Korteweg (NSK) equations, which supplement the EK-equations with a viscous term and take the capillarity coefficient κ as a constant, the absence of dissipative regularization (parabolic smoothing) imposes problems in the analytical research as well as in numerical computations. Hence, it is a challenge to design energy conservative, stable and high order accurate numerical discretizations for the EK-equations.

Due to the ubiquitousness in mathematical physics of the EK-equations equipped with various choices of κ and F (or p), there have been many analytical studies for the EK-equations in the past decades. The investigation of the Cauchy problem for the general EK-equations in one dimension dates back to Benzoni-Garage et al. [6]. Later, they generalized the local well-posedness results to any dimension by a suitably extended formulation of the EK-equations [7]. They also studied the existence and stability of solitons and kinks using Hamiltonian structures and phase portrait analysis of the governing ordinary differential equations (ODEs) in [8]. Antonelli et al. considered in [1] the global existence of weak solutions to a class of QHD equations by taking advantage of the equivalence of the QHD equations with the nonlinear Schrödinger (NLS) equation via the so-called Madelung transform. To extend this result to more general capillarity coefficients κ, Giesselmann [23] and Bresch, [11] respectively, developed the relative entropy methods that are used to prove the existence of global weak solutions of the EK-equations. Under a natural stability condition on the pressure, Audiard [4] proved the existence of global strong solutions of the EK-equations for small irrotational data in dimension at least three. Later, he obtained a lower bound on the time of existence of the solution that depends only on the rotational part, provided that the initial velocity has a small rotational part [3]. Recently Antonelli et al. proved the global existence of finite energy weak solutions of NSK equations for large initial data in [2].

In the past two decades, many numerical methods have been developed for the computation of the (non-)isothermal NSK equations and EK-equations with a constant capillarity coefficient. For example, Giesselmann considered a discontinuous Galerkin (DG) method combined with a second-order accurate Crank-Nicolson type time discretization in [24] for the NSK equations and the EK-equations with a constant capillarity coefficient. The resulting scheme for the NSK equations is mass conservative and energy dissipa-

tive, and the scheme for the EK-equations is mass and energy conservative. Recently in [16] Dhaouadi and Dumbser first presented a novel first-order hyperbolic reformulation, which is based on a combination of the first-order hyperbolic Godunov-Peshkov-Romenski model of continuum mechanics with an augmented Lagrangian approach of the NSK equations. Then the governing PDEs are solved with a high order ADER DG method with a posteriori subcell finite volume limiter in case of discontinuities. They showed arbitrary high order accuracy of the scheme, but did not prove the energy dissipation property. One can refer to [9, 13, 19, 25, 30, 33, 35, 41, 43, 44, 46, 47] for other numerical methods solving the NSK equations. However, only a few authors have considered the numerical solution of the EK-equations with a variable capillarity coefficient. Hoefer et al. [31] considered the quantum fluid Bose-Einstein condensate and numerically simulated the governing Gross-Pitaevskii (GP) equation, which can be converted into the QHD equations via the Madelung transform. They found that the experimentally observed ripples correspond to the dispersive shock waves of the GP equation. Under the assumption $p'(\rho) > 0$, Noble and Vila [42] studied the stability of various difference approximations of the one-dimensional EK-equations, and obtained several stable schemes in the Von Neumann sense and entropy stable schemes under suitable Courant-Friedrichs-Levy (CFL) condition. Later, Bresch et al. [10] generalized the entropy stable schemes to multi-dimension based on a generalization of the quantum Bohm potential identity. In [15, 17, 18] Dhaouadi, Favrie, Gavrilyuk and Vila presented an augmented Lagrangian approach for the EK-equations. They first derived a first-order hyperbolic model with stiff source terms, which approximates the EK-equations through an augmented Lagrangian, and then applied the finite volume method to solve the augmented EK equations.

The numerical discretizations mentioned above for the truly general EK-equations with a variable capillarity coefficient assume that the first-order part is hyperbolic (or constructs a hyperbolic approximation) and implement first or second-order finite difference or finite volume methods. As a comparison, the LDG method is high-order accurate and has excellent flexibility in dealing with the highly nonlinear terms in the EK-equations by carefully introducing auxiliary variables. This motivated us to develop an energy conservative scheme, which can preserve the total energy $\mathcal{H}$ of the general EK-equations in a discrete way. Also, an energy conservative LDG discretization is developed for the EK-equations for the special case when the velocity field is irrotational. It should be emphasized here that no assumptions are made in the numerical discretization on the pressure function p (or the free energy density F). When coupled with the SDC time integration methods, both schemes are arbitrary high-order as long as suitable numerical fluxes are adopted. The LDG method as an extension of the DG method was initially developed to solve the nonlinear convection-diffusion equations by Cockburn and Shu [14], later this technique was implemented to solve nonlinear KdV type equations [58], Camassa-Holm equation [53], Degasperis-Procesi equation [55], NSK equations with constant capillarity [46,47], Serre equations [61] and many other partial differential equations (PDEs) containing high-order spatial derivatives. For a detailed description and review of the LDG

method, we refer to [54] and the references therein.

The application of LDG methods to the EK-equations will generate a large coupled system of ODEs, which require accurate and efficient time integration methods to march in time. Explicit time discretizations will suffer from the extremely small time step restriction $\mathcal{O}(h^3)$ for stability, due to the existence of the third-order derivative of the density in the capillary term. Fully implicit time marching techniques require the computation of a Jacobian matrix, and it is non-trivial to deal with the strong nonlinearity in the EK-equations. Since they were proposed by Minion [40], traditional semi-implicit SDC methods have been adopted to solve nonlinear problems [21, 29, 51] that contain easily separable stiff and non-stiff components. Owing to the difficulty of separating the variable capillarity $\kappa(\rho)$ and the derivatives of density $\nabla\rho$, $\Delta\rho$ in the Korteweg term, we will adopt in this paper the novel semi-implicit SDC time marching methods presented in [28], which can treat ODEs without explicitly separating the equations into stiff and non-stiff components.

The organization of the paper is as follows. Notations and some auxiliary results are presented in Section 2. In Section 3, we develop an LDG discretization for the general EK-equations, namely the energy conservative scheme GEK-C, and prove the discrete energy conservation property. Under the assumption of an irrotational velocity field, we also present a relatively simple LDG discretization, namely the IEK-C scheme, which is especially suitable for the QHD equations and discussed in Section 4. In Section 5, we first present the two fully discrete schemes by combining the spatial discretization with a first-order accurate time discretization, which is then extended to the semi-implicit SDC methods to achieve uniform high-order accuracy. Section 6 contains numerical experiments illustrating the performance of the presented methods. Finally, we state some conclusions in Section 7.

2 Notations and auxiliary results

Let $\mathcal{T}_h=\{K\}$ be a shape regular tessellation of the domain Ω such that $\bigcup_{K\in\mathcal{T}_h}\overline{K}\to\overline{\Omega}$ as $h\to 0$, with $h:=\max_{K\in\mathcal{T}_h}h_K$ the mesh size and h_K the diameter of element K. For each $K\in\mathcal{T}_h$, we denote by $\mathbf{n}_K$ the unit outward normal vector to the boundary ∂K. We also denote by Γ the union of the faces of all elements K, i.e., $\Gamma=\bigcup_{K\in\mathcal{T}_h}\partial K$, and classify them into internal and boundary faces, i.e., $\Gamma=\Gamma_I\cup\Gamma_B$. What should be emphasized is that a periodic boundary face is treated as an internal face.

To introduce the flux functions, let $e\in\Gamma$ be a face shared by the "left" and "right" elements K_L and K_R, i.e., $e=\partial K_L\cap\partial K_R$, where the so-called "left" and "right" can be uniquely defined for each internal face $e\in\Gamma_I$ according to any fixed rule, and for a boundary face $e\in\Gamma_B$, we assign K_L and K_R (a ghost element) to lie, respectively, interior and exterior to the domain Ω. Suppose ϕ is a function on K_L and K_R, which could be discontinuous across e, then we define ϕ^L and ϕ^R as $(\phi|_{K_L})|_e$ and $(\phi|_{K_R})|_e$, the left and right traces, respectively. Similar definitions can be obtained component-wisely for vector-valued and

matrix-valued functions.

Next, we define the average and jump operators. To this end, let ϕ, $\mathbf{v}$ and $\underline{\tau}$ be scalar-valued, vector-valued and matrix-valued functions, respectively, and $\mathbf{x}$ be an arbitrary point at the face $e=\partial K_L\cap\partial K_R$. Denote by $\mathbf{n}_L$ and $\mathbf{n}_R$ the unit normal vectors at $\mathbf{x}$ pointing exterior to K_L and K_R, respectively, with $\mathbf{n}_L+\mathbf{n}_R=\mathbf{0}$. If $e\in\Gamma_I$ is an internal face, then the averages and jumps of, respectively, scalar, vector and matrix-valued functions ϕ, $\mathbf{v}$ and $\underline{\tau}$ at $\mathbf{x}\in e$ are defined by

$$\begin{aligned}
&\{\phi\}:=\frac{1}{2}(\phi^L+\phi^R),\quad [\phi]:=\phi^L\mathbf{n}_L+\phi^R\mathbf{n}_R,\\
&\{\mathbf{v}\}:=\frac{1}{2}(\mathbf{v}^L+\mathbf{v}^R),\quad [\mathbf{v}]:=\mathbf{v}^L\cdot\mathbf{n}_L+\mathbf{v}^R\cdot\mathbf{n}_R,\quad [\mathbf{v}]_*:=\mathbf{v}^L\otimes\mathbf{n}_L+\mathbf{v}^R\otimes\mathbf{n}_R,\\
&\{\underline{\tau}\}:=\frac{1}{2}(\underline{\tau}^L+\underline{\tau}^R),\quad [\underline{\tau}]:=\underline{\tau}^L\mathbf{n}_L+\underline{\tau}^R\mathbf{n}_R.
\end{aligned}$$

On a boundary face $e\in\Gamma_B$, we set

$$\begin{aligned}
&\{\phi\}:=\phi^L,\quad [\phi]:=\phi^L\mathbf{n}_L,\\
&\{\mathbf{v}\}:=\mathbf{v}^L,\quad [\mathbf{v}]:=\mathbf{v}^L\cdot\mathbf{n}_L,\quad [\mathbf{v}]_*:=\mathbf{v}^L\otimes\mathbf{n}_L,\\
&\{\underline{\tau}\}:=\underline{\tau}^L,\quad [\underline{\tau}]:=\underline{\tau}^L\mathbf{n}_L.
\end{aligned}$$

Note that the jumps of a scalar-valued function ϕ and a matrix-valued function $\underline{\tau}$ are both vector-valued functions. As for the vector-valued function $\mathbf{v}$, we define two jumps $[\mathbf{v}]$ and $[\mathbf{v}]_*$, which are scalar-valued and matrix-valued functions, respectively. Moreover, we will define the notation $[\![\cdot]\!]$ at $\mathbf{x}\in e$ as

$$[\![\phi]\!]=\phi^R-\phi^L,\quad [\![\mathbf{v}]\!]=\mathbf{v}^R-\mathbf{v}^L,\quad [\![\underline{\tau}]\!]=\underline{\tau}^R-\underline{\tau}^L,$$

if $e\in\Gamma_I$. On a boundary face $e\in\Gamma_B$, we set

$$[\![\phi]\!]=-\phi^L,\quad [\![\mathbf{v}]\!]=-\mathbf{v}^L,\quad [\![\underline{\tau}]\!]=-\underline{\tau}^L.$$

Each element K of the tessellation $\mathcal{T}_h$ is connected to a reference element $\hat{K}$ through some mapping $F_K:\hat{K}\to K$. Then the finite element spaces associated with the tessellation $\mathcal{T}_h$ are given by

$$\begin{aligned}
&V_h^k=\left\{v\in L^2(\Omega):v|_K\circ F_K\in\mathcal{P}(\hat{K}),\ \forall K\in\mathcal{T}_h\right\},\\
&\Sigma_h^k=\left\{\mathbf{v}=(v_1,\cdots,v_d)^T\in(L^2(\Omega))^d:v_i|_K\circ F_K\in\mathcal{P}(\hat{K}),\ i=1,\cdots,d,\ \forall K\in\mathcal{T}_h\right\},
\end{aligned}$$

with $\mathcal{P}(\hat{K})=P^k(\hat{K})$ or $Q^k(\hat{K})$, the space of polynomials on the reference element $\hat{K}$ of maximum degree k with respect to all d variables or each variable, respectively.

To present the DG schemes in a compact way, we define the discrete inner products

$$(\phi,\varphi):=\sum_{K\in\mathcal{T}_h}(\phi,\varphi)_K,\quad (\mathbf{v},\mathbf{w}):=\sum_{K\in\mathcal{T}_h}(\mathbf{v},\mathbf{w})_K,\quad (\underline{\tau},\underline{\sigma}):=\sum_{K\in\mathcal{T}_h}(\underline{\tau},\underline{\sigma})_K,$$

with

$$(\phi,\varphi)_K := \int_K \phi\psi d\mathbf{x}, \quad (\mathbf{v},\mathbf{w})_K := \int_K \mathbf{v}\cdot\mathbf{w} d\mathbf{x}, \quad (\underline{\tau},\underline{\sigma})_K := \int_K \underline{\tau}:\underline{\sigma} d\mathbf{x},$$

for the scalar-valued functions ϕ, φ, vector-valued functions $\mathbf{v}$, $\mathbf{w}$ and matrix-valued functions $\underline{\tau}$, $\underline{\sigma}$, respectively. We also introduce the DG discretization operators

$$\mathcal{D}^1(\phi,\mathbf{w};\widehat{\phi}) := \sum_{K\in\mathcal{T}_h} \mathcal{D}^1_K(\phi,\mathbf{w};\widehat{\phi}), \qquad \mathcal{D}^2(\mathbf{v},\varphi;\widehat{\mathbf{v}}) := \sum_{K\in\mathcal{T}_h} \mathcal{D}^2_K(\mathbf{v},\varphi;\widehat{\mathbf{v}}),$$
$$\mathcal{D}^3(\mathbf{v},\underline{\sigma};\widehat{\mathbf{v}}) := \sum_{K\in\mathcal{T}_h} \mathcal{D}^3_K(\mathbf{v},\underline{\sigma};\widehat{\mathbf{v}}), \qquad \mathcal{D}^4(\underline{\tau},\mathbf{w};\widehat{\underline{\tau}}) := \sum_{K\in\mathcal{T}_h} \mathcal{D}^4_K(\underline{\tau},\mathbf{w};\widehat{\underline{\tau}}),$$

with

$$\begin{aligned}
\mathcal{D}^1_K(\phi,\mathbf{w};\widehat{\phi}) &:= -\int_K \phi\nabla\cdot\mathbf{w} d\mathbf{x} + \int_{\partial K} \widehat{\phi}\mathbf{w}^-\cdot\mathbf{n}_K ds,\\
\mathcal{D}^2_K(\mathbf{v},\varphi;\widehat{\mathbf{v}}) &:= -\int_K \mathbf{v}\cdot\nabla\varphi d\mathbf{x} + \int_{\partial K} \widehat{\mathbf{v}}\cdot\mathbf{n}_K\varphi^- ds,\\
\mathcal{D}^3_K(\mathbf{v},\underline{\sigma};\widehat{\mathbf{v}}) &:= -\int_K \mathbf{v}\cdot\nabla\cdot\underline{\sigma} d\mathbf{x} + \int_{\partial K} \underline{\sigma}^-\mathbf{n}_K\cdot\widehat{\mathbf{v}} ds,\\
\mathcal{D}^4_K(\underline{\tau},\mathbf{w};\widehat{\underline{\tau}}) &:= -\int_K \underline{\tau}:\nabla\mathbf{w} d\mathbf{x} + \int_{\partial K} \widehat{\underline{\tau}}\mathbf{n}_K\cdot\mathbf{w}^- ds,
\end{aligned}$$

as well as

$$\widetilde{\mathcal{D}}^1(\phi,\mathbf{w};\alpha) := \sum_{K\in\mathcal{T}_h} \widetilde{\mathcal{D}}^1_K(\phi,\mathbf{w};\alpha), \qquad \widetilde{\mathcal{D}}^2(\mathbf{v},\varphi;\alpha) := \sum_{K\in\mathcal{T}_h} \widetilde{\mathcal{D}}^2_K(\mathbf{v},\varphi;\alpha),$$
$$\widetilde{\mathcal{D}}^3(\mathbf{v},\underline{\sigma};\alpha) := \sum_{K\in\mathcal{T}_h} \widetilde{\mathcal{D}}^3_K(\mathbf{v},\underline{\sigma};\alpha), \qquad \widetilde{\mathcal{D}}^4(\underline{\tau},\mathbf{w};\alpha) := \sum_{K\in\mathcal{T}_h} \widetilde{\mathcal{D}}^4_K(\underline{\tau},\mathbf{w};\alpha),$$

with

$$\widetilde{\mathcal{D}}^1_K(\phi,\mathbf{w};\alpha) := \mathcal{D}^1_K(\phi,\mathbf{w};\{\phi\}+\alpha[\![\phi]\!]), \qquad \widetilde{\mathcal{D}}^2_K(\mathbf{v},\varphi;\alpha) := \mathcal{D}^2_K(\mathbf{v},\varphi;\{\mathbf{v}\}+\alpha[\![\mathbf{v}]\!]),$$
$$\widetilde{\mathcal{D}}^3_K(\mathbf{v},\underline{\sigma};\alpha) := \mathcal{D}^3_K(\mathbf{v},\underline{\sigma};\{\mathbf{v}\}+\alpha[\![\mathbf{v}]\!]), \qquad \widetilde{\mathcal{D}}^4_K(\underline{\tau},\mathbf{w};\alpha) := \mathcal{D}^4_K(\underline{\tau},\mathbf{w};\{\underline{\tau}\}+\alpha[\![\underline{\tau}]\!]),$$

and $\alpha\in[-\frac{1}{2},\frac{1}{2}]$. Here ":" is the summation of the element-wise product of two matrices. Suppose $\underline{a}=(a_{ij})$, $\underline{b}=(b_{ij})$, then $\underline{a}:\underline{b}=\sum_{ij}a_{ij}b_{ij}$. The superscript in φ^-, $\mathbf{w}^-$ and $\underline{\sigma}^-$ means taking value at ∂K from within the interior of element K. Similarly, in the following section, we will use the notations φ^+, $\mathbf{w}^+$ and $\underline{\sigma}^+$ to denote values from within the interior of the element adjacent to K. Clearly, $\alpha=\pm\frac{1}{2}$ and $\alpha=0$ lead to the alternating fluxes and central fluxes, respectively.

Using the above definitions, we have the following lemmas.

Lemma 2.1. *For any face $e=\partial K_L\cap\partial K_R$ (K_R may be a ghost element), we have*

$$(\{\phi\}+\alpha[\![\phi]\!])[\mathbf{v}]+(\{\mathbf{v}\}-\alpha[\![\mathbf{v}]\!])\cdot[\phi]=[\phi\mathbf{v}]. \tag{2.1}$$

Proof. Suppose $e\in\Gamma_I$ is an internal face, it is easy to check that

$$\phi^L[\mathbf{v}]+\mathbf{v}^R\cdot[\phi]=[\phi\mathbf{v}],\quad \phi^R[\mathbf{v}]+\mathbf{v}^L\cdot[\phi]=[\phi\mathbf{v}],\quad \{\phi\}[\mathbf{v}]+\{\mathbf{v}\}\cdot[\phi]=[\phi\mathbf{v}].$$

Hence, expanding the left hand side of equality (2.1) yields

$$\begin{aligned}&\{\phi\}[\mathbf{v}]+\{\mathbf{v}\}\cdot[\phi]+\alpha\left(\phi^R[\mathbf{v}]+\mathbf{v}^L\cdot[\phi]\right)-\alpha\left(\phi^L[\mathbf{v}]+\mathbf{v}^R\cdot[\phi]\right)\\ =&[\phi\mathbf{v}]+\alpha[\phi\mathbf{v}]-\alpha[\phi\mathbf{v}]=[\phi\mathbf{v}].\end{aligned}$$

The case for a boundary face $e\in\Gamma_B$ can be verified in a similar procedure. □

Lemma 2.2. *For periodic boundary conditions and any scalar-valued function ϕ, vector-valued function $\mathbf{v}$ and $\alpha\in[-\frac{1}{2},\frac{1}{2}]$, there holds*

$$\widetilde{\mathcal{D}}^1(\phi,\mathbf{v};\alpha)+\widetilde{\mathcal{D}}^2(\mathbf{v},\phi;-\alpha)=0. \tag{2.2}$$

Proof. Expanding the left hand side of (2.2), we obtain

$$\begin{aligned}&\widetilde{\mathcal{D}}^1(\phi,\mathbf{v};\alpha)+\widetilde{\mathcal{D}}^2(\mathbf{v},\phi;-\alpha)\\ =&\sum_{K\in\mathcal{T}_h}\left(-\int_K(\phi\nabla\cdot\mathbf{v}+\mathbf{v}\cdot\nabla\phi)\,d\mathbf{x}+\int_{\partial K}\left((\{\phi\}+\alpha[\![\phi]\!])\mathbf{v}^-\cdot\mathbf{n}_K+(\{\mathbf{v}\}-\alpha[\![\mathbf{v}]\!])\cdot\mathbf{n}_K\phi^-\right)ds\right)\\ =&\sum_{e\in\Gamma_I}\int_e(-[\phi\mathbf{v}]+(\{\phi\}+\alpha[\![\phi]\!])[\mathbf{v}]+(\{\mathbf{v}\}-\alpha[\![\mathbf{v}]\!])\cdot[\phi])\,ds=0,\end{aligned}$$

where we have used the divergence theorem and Lemma 2.1. □

Lemma 2.3. *For periodic boundary conditions and any scalar-valued function ϕ, vector-valued function $\mathbf{v}$ and $\alpha\in[-\frac{1}{2},\frac{1}{2}]$, there holds*

$$\mathcal{D}^4(\phi\mathbf{v}\otimes\mathbf{v},\mathbf{v};\widehat{\phi\mathbf{v}\otimes\mathbf{v}})-\widetilde{\mathcal{D}}^2\left(\phi\mathbf{v},\frac{1}{2}|\mathbf{v}|^2;\alpha\right)=0, \tag{2.3}$$

with $\widehat{\phi\mathbf{v}\otimes\mathbf{v}}=\{\mathbf{v}\}\otimes(\{\phi\mathbf{v}\}+\alpha[\![\phi\mathbf{v}]\!])$.

Proof. Expanding the terms in (2.3) yields

$$\begin{aligned}&\sum_K\left(\int_K-\phi\mathbf{v}\otimes\mathbf{v}:\nabla\mathbf{v}+\phi\mathbf{v}\cdot\nabla\left(\frac{1}{2}|\mathbf{v}|^2\right)d\mathbf{x}\right.\\ &\quad\left.+\int_{\partial K}(\widehat{\phi\mathbf{v}\otimes\mathbf{v}})\mathbf{n}_K\cdot\mathbf{v}^--(\{\phi\mathbf{v}\}+\alpha[\![\phi\mathbf{v}]\!])\cdot\mathbf{n}_K\left(\frac{1}{2}|\mathbf{v}^-|^2\right)ds\right)\\ =&\sum_K\int_K-\phi\mathbf{v}^T(\nabla\mathbf{v})\mathbf{v}+\phi\mathbf{v}^T(\nabla\mathbf{v})^T\mathbf{v}\,d\mathbf{x}\\ &\quad+\sum_e\int_e(\{\mathbf{v}\}\otimes(\{\phi\mathbf{v}\}+\alpha[\![\phi\mathbf{v}]\!])):[\mathbf{v}]_*-(\{\phi\mathbf{v}\}+\alpha[\![\phi\mathbf{v}]\!])\cdot\left[\frac{1}{2}|\mathbf{v}|^2\right]ds.\end{aligned}$$

Note that

$$\phi\mathbf{v}^T(\nabla\mathbf{v})^T\mathbf{v}=\phi\mathbf{v}^T(\nabla\mathbf{v})\mathbf{v},$$

and

$$\begin{aligned}(\{\mathbf{v}\}\otimes(\{\phi\mathbf{v}\}+\alpha_1[\![\phi\mathbf{v}]\!])):[\mathbf{v}]_*&=\Big((\mathbf{v}^L-\mathbf{v}^R)^T\{\mathbf{v}\}\Big)\Big((\{\phi\mathbf{v}\}+\alpha_1[\![\phi\mathbf{v}]\!])^T\mathbf{n}_L\Big)\\&=(\{\phi\mathbf{v}\}+\alpha_1[\![\phi\mathbf{v}]\!])\cdot\Big[\frac{1}{2}|\mathbf{v}|^2\Big],\end{aligned}$$

hence equality (2.3) holds. □

3 LDG discretization for the general EK-equations

In this section, we will present a semi-discrete LDG discretization for the general EK-equations in multidimension. We leave the time dependence continuous. The LDG discretization is based on a hybrid form of the EK-equations and will be proven to be energy conservative. To this end, we consider the following hybrid form of the EK-equations

$$\rho_t+\nabla\cdot(\rho\mathbf{u})=0, \tag{3.1a}$$

$$(\rho\mathbf{u})_t+\nabla\cdot(\rho\mathbf{u}\otimes\mathbf{u})+\rho\nabla F'(\rho)=\rho\nabla\left(\kappa(\rho)\Delta\rho+\frac{1}{2}\kappa'(\rho)|\nabla\rho|^2\right), \tag{3.1b}$$

by combining the conservative form (1.1) and the non-conservative form (1.3). Compared with (1.3), the main difference is that we leave the term $\nabla\cdot(\rho\mathbf{u}\otimes\mathbf{u})$ in (3.1) in a conservative form. Using the method of lines and rewriting (3.1) as

$$\rho_t+\nabla\cdot(\rho\mathbf{u})=0, \tag{3.2a}$$

$$\mathbf{m}_t+\nabla\cdot(\rho\mathbf{u}\otimes\mathbf{u})+\rho\nabla\Big(f-r+s+\frac{1}{2}|\mathbf{u}|^2\Big)=\mathbf{0}, \tag{3.2b}$$

$$r-\nabla\cdot\mathbf{w}=0,\quad \mathbf{q}-\nabla\rho=\mathbf{0},\quad \rho\mathbf{u}-\mathbf{m}=\mathbf{0}, \tag{3.2c}$$

$$f-F'(\rho)+\frac{1}{2}|\mathbf{u}|^2=0,\quad s-\frac{1}{2}\kappa'(\rho)|\mathbf{q}|^2=0,\quad \mathbf{w}-\kappa(\rho)\mathbf{q}=\mathbf{0}, \tag{3.2d}$$

which contain only first-order spatial derivatives. The conservative LDG discretization denoted GEK-C is based on the weak formulation of (3.2), which is obtained by multiplying (3.2) with arbitrary test functions, integration by parts of each element and summing all contributions from elements and faces. The LDG discretization is: find ρ_h, f_h, s_h, $r_h\in V_h^k$, $\mathbf{u}_h$, $\mathbf{m}_h$, $\mathbf{q}_h$, $\mathbf{w}_h\in\Sigma_h^k$, such that, for all test functions ϕ, θ, ζ, $\mu\in V_h^k$, $\boldsymbol{\psi}$, $\boldsymbol{\xi}$, $\boldsymbol{\eta}$, $\boldsymbol{\nu}\in\Sigma_h^k$,

the following equations are satisfied,

$$((\rho_h)_t,\phi)+\mathcal{D}^2(\rho_h\mathbf{u}_h,\phi;\widehat{\rho_h\mathbf{u}_h})=0, \tag{3.3a}$$

$$((\mathbf{m}_h)_t,\boldsymbol{\psi})+\mathcal{D}^4(\rho_h\mathbf{u}_h\otimes\mathbf{u}_h,\boldsymbol{\psi};\widehat{\rho_h\mathbf{u}_h\otimes\mathbf{u}_h}) - \mathcal{D}^2\Big(\rho_h\boldsymbol{\psi},f_h-r_h+s_h+\frac{1}{2}|\mathbf{u}_h|^2;\widehat{\rho_h\boldsymbol{\psi}}\Big)=0, \tag{3.3b}$$

$$(r_h,\theta)-\mathcal{D}^2(\mathbf{w}_h,\theta;\widehat{\mathbf{w}_h})=0, \tag{3.3c}$$

$$(\mathbf{q}_h,\boldsymbol{\xi})-\mathcal{D}^1(\rho_h,\boldsymbol{\xi};\widehat{\rho_h})=0, \tag{3.3d}$$

$$(\rho_h\mathbf{u}_h,\boldsymbol{\eta})-(\mathbf{m}_h,\boldsymbol{\eta})=0, \tag{3.3e}$$

$$(f_h,\zeta)-\Big(F'(\rho_h)-\frac{1}{2}|\mathbf{u}_h|^2,\zeta\Big)=0, \tag{3.3f}$$

$$(s_h,\mu)-\frac{1}{2}(\kappa'(\rho_h)|\mathbf{q}_h|^2,\mu)=0, \tag{3.3g}$$

$$(\mathbf{w}_h,\boldsymbol{\nu})-(\kappa(\rho_h)\mathbf{q}_h,\boldsymbol{\nu})=0. \tag{3.3h}$$

All equations in (3.3) can be obtained by a simple integration by parts, except for the last term in (3.3b), which is discussed in Appendix A. The following numerical fluxes

$$\widehat{\rho_h\mathbf{u}_h}=\{\rho_h\mathbf{u}_h\}+\alpha_1[\![\rho_h\mathbf{u}_h]\!],\quad \widehat{\rho_h\mathbf{u}_h\otimes\mathbf{u}_h}=\{\mathbf{u}_h\}\otimes\widehat{\rho_h\mathbf{u}_h}, \tag{3.4a}$$

$$\widehat{\rho_h\boldsymbol{\psi}}=\{\rho_h\boldsymbol{\psi}\}+\alpha_1[\![\rho_h\boldsymbol{\psi}]\!],\quad \widehat{\rho_h}=\{\rho_h\}+\alpha_2[\![\rho_h]\!],\quad \widehat{\mathbf{w}_h}=\{\mathbf{w}_h\}-\alpha_2[\![\mathbf{w}_h]\!], \tag{3.4b}$$

with $\alpha_1,\alpha_2\in[-\frac{1}{2},\frac{1}{2}]$, will ensure that the LDG discretization is energy conservative.

Next, we prove the energy conservation property of the GEK-C LDG discretization.

Proposition 3.1. *For periodic boundary conditions, solutions to the GEK-C LDG discretization* (3.3) *with numerical fluxes* (3.4) *satisfy*

$$\frac{d}{dt}\int_\Omega\left(\frac{1}{2}\rho_h|\mathbf{u}_h|^2+F(\rho_h)+\frac{1}{2}\kappa(\rho_h)|\mathbf{q}_h|^2\right)d\mathbf{x}=0. \tag{3.5}$$

Proof. Taking the time derivative of (3.3d) and (3.3e), and choosing the test functions

$$\phi=f_h-r_h+s_h,\quad \boldsymbol{\psi}=\mathbf{u}_h,\quad \theta=(\rho_h)_t,\quad \boldsymbol{\xi}=\mathbf{w}_h,$$
$$\boldsymbol{\eta}=\mathbf{u}_h,\quad \zeta=-(\rho_h)_t,\quad \mu=-(\rho_h)_t,\quad \boldsymbol{\nu}=-(\mathbf{q}_h)_t,$$

we have

$$((\rho_h)_t,f_h-r_h+s_h)+\widetilde{\mathcal{D}}^2(\rho_h\mathbf{u}_h,f_h-r_h+s_h;\alpha_1)=0, \tag{3.6a}$$

$$((\mathbf{m}_h)_t,\mathbf{u}_h)+\mathcal{D}^4(\rho_h\mathbf{u}_h\otimes\mathbf{u}_h,\mathbf{u}_h;\widehat{\rho_h\mathbf{u}_h\otimes\mathbf{u}_h})-\widetilde{\mathcal{D}}^2\Big(\rho_h\mathbf{u}_h,f_h-r_h+s_h+\frac{1}{2}|\mathbf{u}_h|^2;\alpha_1\Big)=0, \tag{3.6b}$$

$$(r_h,(\rho_h)_t)-\widetilde{\mathcal{D}}^2(\mathbf{w}_h,(\rho_h)_t;-\alpha_2)=0,\quad((\mathbf{q}_h)_t,\mathbf{w}_h)-\widetilde{\mathcal{D}}^1((\rho_h)_t,\mathbf{w}_h;\alpha_2)=0, \tag{3.6c}$$

$$((\rho_h)_t\mathbf{u}_h+\rho_h(\mathbf{u}_h)_t,\mathbf{u}_h)-((\mathbf{m}_h)_t,\mathbf{u}_h)=0,\ -(f_h,(\rho_h)_t)+\Big(F'(\rho_h)-\frac{1}{2}|\mathbf{u}_h|^2,(\rho_h)_t\Big)=0, \tag{3.6d}$$

$$-(s_h,(\rho_h)_t)+\frac{1}{2}(\kappa'(\rho_h)|\mathbf{q}_h|^2,(\rho_h)_t)=0,\quad-(\mathbf{w}_h,(\mathbf{q}_h)_t)+(\kappa(\rho_h)\mathbf{q}_h,(\mathbf{q}_h)_t)=0. \tag{3.6e}$$

Summing up all equations in (3.6) and using the identities

$$\widetilde{\mathcal{D}}^1((\rho_h)_t,\mathbf{w}_h;\alpha_2)+\widetilde{\mathcal{D}}^2(\mathbf{w}_h,(\rho_h)_t;-\alpha_2)=0, \tag{3.7a}$$

$$\mathcal{D}^4(\rho_h\mathbf{u}_h\otimes\mathbf{u}_h,\mathbf{u}_h;\rho_h\widehat{\mathbf{u}_h\otimes\mathbf{u}_h})-\widetilde{\mathcal{D}}^2\Big(\rho_h\mathbf{u}_h,\frac{1}{2}|\mathbf{u}_h|^2;\alpha_1\Big)=0, \tag{3.7b}$$

which follow from Lemmas 2.2 and 2.3, we obtain

$$\Big(\frac{1}{2}|\mathbf{u}_h|^2+F'(\rho_h)+\frac{1}{2}\kappa'(\rho_h)|\mathbf{q}_h|^2,(\rho_h)_t\Big)+(\rho_h\mathbf{u}_h,(\mathbf{u}_h)_t)+(\kappa(\rho_h)\mathbf{q}_h,(\mathbf{q}_h)_t)=0,$$

which gives (3.5). □

Remark 3.1. The energy conservation property of the GEK-C LDG discretization and the IEK-C LDG discretization introduced in Section 4 remains valid for boundary conditions

$$\frac{\partial\rho}{\partial\mathbf{n}}=0,\quad\mathbf{u}=\mathbf{0}\quad\text{on }\partial\Omega.$$

This conclusion follows directly from equalities in (3.7) and (4.10) since all the boundary face contributions vanish in this case.

4 Special discretization for potential flow

The GEK-C LDG discretization discussed in Section 3 is valid for the general EK-equations without considering whether the velocity field is rotational or not. For some important applications, such as the QHD equations, we only have to consider an irrotational (potential flow) velocity field. Considering the importance of the QHD equations, we will discuss a special LDG discretization suitable for the EK-equations with an irrotational velocity field in this section. This LDG discretization is considerably simpler than the GEK-C LDG discretization for the general EK-equations.

4.1 Madelung transform

In this section, we will start with the introduction of the Madelung transform. For the semi-classical NLS equation [12]:

$$i\varepsilon\psi_t+\frac{\varepsilon^2}{2}\Delta\psi=g(|\psi|^2)\psi, \tag{4.1}$$

we seek solutions of (4.1) of the form

$$\psi(\mathbf{x},t)=\sqrt{\rho(\mathbf{x},t)}e^{\frac{i}{\varepsilon}\phi(\mathbf{x},t)}, \tag{4.2}$$

where $\rho(\mathbf{x},t)\geq 0$ and $\phi(\mathbf{x},t)$ are real-valued functions that represent the square of the modulus and the argument of $\psi(\mathbf{x},t)$, respectively. The relation (4.2) is the so-called Madelung transform introduced in [38]. For (4.2) we can obtain

$$\psi_t=\left(\frac{\rho_t}{2\rho}+\frac{i}{\varepsilon}\phi_t\right)\psi, \tag{4.3a}$$

$$\Delta\psi=\left(\frac{\Delta\sqrt{\rho}}{\sqrt{\rho}}+\frac{i}{\varepsilon\rho}\nabla\cdot(\rho\nabla\phi)-\frac{1}{\varepsilon^2}|\nabla\phi|^2\right)\psi. \tag{4.3b}$$

Substituting (4.3) into (4.1) gives

$$\frac{i\varepsilon}{2\rho}(\rho_t+\nabla\cdot(\rho\nabla\phi))+\left(-\phi_t-\frac{1}{2}|\nabla\phi|^2-g(\rho)+\frac{\varepsilon^2}{2}\frac{\Delta\sqrt{\rho}}{\sqrt{\rho}}\right)=0. \tag{4.4}$$

Using $\mathbf{u}=\nabla\phi$ in (4.4) then gives the hydrodynamic form of the NLS equation (4.1)

$$\rho_t+\nabla\cdot(\rho\mathbf{u})=0, \tag{4.5a}$$

$$\mathbf{u}_t+\mathbf{u}\cdot\nabla\mathbf{u}+\nabla g(\rho)=\frac{\varepsilon^2}{2}\nabla\left(\frac{\Delta\sqrt{\rho}}{\sqrt{\rho}}\right). \tag{4.5b}$$

Formulation (4.5) of the NLS equation is also referred to as the Madelung equations or QHD equations. More importantly, they represent a particular case of the EK-equations with

$$F(\rho)=\int^{\rho} g(\rho)\,d\rho,\quad \kappa(\rho)=\frac{\varepsilon^2}{4\rho}\quad\text{and}\quad \nabla\times\mathbf{u}=\mathbf{0}.$$

4.2 LDG discretization for the EK-equations with irrotational velocity field

For an irrotational velocity field, hence $\nabla\times\mathbf{u}=\mathbf{0}$, we have the relation

$$\mathbf{u}\cdot\nabla\mathbf{u}=\frac{1}{2}\nabla|\mathbf{u}|^2.$$

We can rewrite the non-conservative form of the EK-equations (1.3) for an irrotational flow then as the first order system

$$\rho_t+\nabla\cdot\mathbf{m}=0,\quad \mathbf{u}_t+\nabla(f-r+s)=\mathbf{0},\quad r-\nabla\cdot\mathbf{w}=0,\quad \mathbf{q}-\nabla\rho=\mathbf{0}, \tag{4.6a}$$

$$\mathbf{m}-\rho\mathbf{u}=\mathbf{0},\quad f-\frac{1}{2}|\mathbf{u}|^2-F'(\rho)=0,\quad s-\frac{1}{2}\kappa'(\rho)|\mathbf{q}|^2=0,\quad \mathbf{w}-\kappa(\rho)\mathbf{q}=\mathbf{0}. \tag{4.6b}$$

The conservative LDG discretization, which is denoted IEK-C, for the EK-equations with an irrotational velocity field, is: find ρ_h, f_h, s_h, $r_h \in V_h^k$, $\mathbf{u}_h$, $\mathbf{m}_h$, $\mathbf{q}_h$, $\mathbf{w}_h \in \Sigma_h^k$, such that for all test functions ϕ, θ, ζ, $\mu \in V_h^k$, $\boldsymbol{\psi}$, $\boldsymbol{\xi}$, $\boldsymbol{\eta}$, $\boldsymbol{\nu} \in \Sigma_h^k$, the following equations are satisfied,

$$((\rho_h)_t,\phi)+\mathcal{D}^2(\mathbf{m}_h,\phi;\widehat{\mathbf{m}_h})=0, \tag{4.7a}$$

$$((\mathbf{u}_h)_t,\boldsymbol{\psi})+\mathcal{D}^1(f_h-r_h+s_h,\boldsymbol{\psi};\widehat{f_h-r_h+s_h})=0, \tag{4.7b}$$

$$(r_h,\theta)-\mathcal{D}^2(\mathbf{w}_h,\theta;\widehat{\mathbf{w}_h})=0, \tag{4.7c}$$

$$(\mathbf{q}_h,\boldsymbol{\xi})-\mathcal{D}^1(\rho_h,\boldsymbol{\xi};\widehat{\rho_h})=0, \tag{4.7d}$$

$$(\mathbf{m}_h,\boldsymbol{\eta})-(\rho_h\mathbf{u}_h,\boldsymbol{\eta})=0, \tag{4.7e}$$

$$(f_h,\zeta)-\Big(\frac{1}{2}|\mathbf{u}_h|^2+F'(\rho_h),\zeta\Big)=0, \tag{4.7f}$$

$$(s_h,\mu)-\frac{1}{2}(\kappa'(\rho_h)|\mathbf{q}_h|^2,\mu)=0, \tag{4.7g}$$

$$(\mathbf{w}_h,\boldsymbol{\nu})-(\kappa(\rho_h)\mathbf{q}_h,\boldsymbol{\nu})=0. \tag{4.7h}$$

The use of the L^2 projections (4.7e)-(4.7h) allows to choose test functions equal to $\mathbf{m}_h$, f_h, s_h, $\mathbf{w}_h$, and their linear combinations, since their projections belong to the finite element spaces V_h^k or Σ_h^k. The numerical fluxes are defined as

$$\widehat{f_h-r_h+s_h}=\{f_h-r_h+s_h\}+\alpha_1[\![f_h-r_h+s_h]\!], \tag{4.8a}$$

$$\widehat{\mathbf{m}_h}=\{\mathbf{m}_h\}-\alpha_1[\![\mathbf{m}_h]\!],\quad \widehat{\rho_h}=\{\rho_h\}+\alpha_2[\![\rho_h]\!],\quad \widehat{\mathbf{w}_h}=\{\mathbf{w}_h\}-\alpha_2[\![\mathbf{w}_h]\!], \tag{4.8b}$$

with $\alpha_1,\alpha_2\in[-\frac{1}{2},\frac{1}{2}]$. These fluxes are selected to make the LDG discretization (4.7) satisfy the energy conservation property.

Next, We prove that the IEK-C LDG discretization (4.7) for the EK-equations with an irrotational velocity field is energy conservative.

Proposition 4.1. *For periodic boundary conditions, solutions to the IEK-C LDG discretization* (4.7) *with numerical fluxes* (4.8) *satisfy the energy equality* (3.5).

Proof. Taking the time derivative of (4.7d) and choosing the test functions

$$\phi=f_h-r_h+s_h,\quad \boldsymbol{\psi}=\mathbf{m}_h,\quad \theta=(\rho_h)_t,\quad \boldsymbol{\xi}=\mathbf{w}_h,$$
$$\boldsymbol{\eta}=-(\mathbf{u}_h)_t,\quad \zeta=-(\rho_h)_t,\quad \mu=-(\rho_h)_t,\quad \boldsymbol{\nu}=-(\mathbf{q}_h)_t,$$

we have

$$((\rho_h)_t,f_h-r_h+s_h)+\widetilde{\mathcal{D}}^2(\mathbf{m}_h,f_h-r_h+s_h;-\alpha_1)=0, \tag{4.9a}$$

$$((\mathbf{u}_h)_t,\mathbf{m}_h)+\widetilde{\mathcal{D}}^1(f_h-r_h+s_h,\mathbf{m}_h;\alpha_1)=0, \tag{4.9b}$$

$$(r_h,(\rho_h)_t)-\widetilde{\mathcal{D}}^2(\mathbf{w}_h,(\rho_h)_t;-\alpha_2)=0, \tag{4.9c}$$

$$((\mathbf{q}_h)_t,\mathbf{w}_h)-\widetilde{\mathcal{D}}^1((\rho_h)_t,\mathbf{w}_h;\alpha_2)=0, \tag{4.9d}$$

$$-(\mathbf{m}_h,(\mathbf{u}_h)_t)+(\rho_h\mathbf{u}_h,(\mathbf{u}_h)_t)=0, \tag{4.9e}$$

$$-(f_h,(\rho_h)_t)+\Big(\frac{1}{2}|\mathbf{u}_h|^2+F'(\rho_h),(\rho_h)_t\Big)=0, \tag{4.9f}$$

$$-(s_h,(\rho_h)_t)+\frac{1}{2}(\kappa'(\rho_h)|\mathbf{q}_h|^2,(\rho_h)_t)=0, \tag{4.9g}$$

$$-(\mathbf{w}_h,(\mathbf{q}_h)_t)+(\kappa(\rho_h)\mathbf{q}_h,(\mathbf{q}_h)_t)=0. \tag{4.9h}$$

Summing all contributions in (4.9) and using the identities

$$\widetilde{\mathcal{D}}^1(f_h-r_h+s_h,\mathbf{m}_h;\alpha_1)+\widetilde{\mathcal{D}}^2(\mathbf{m}_h,f_h-r_h+s_h;-\alpha_1)=0, \tag{4.10a}$$

$$\widetilde{\mathcal{D}}^1((\rho_h)_t,\mathbf{w}_h;\alpha_2)+\widetilde{\mathcal{D}}^2(\mathbf{w}_h,(\rho_h)_t;-\alpha_2)=0, \tag{4.10b}$$

which follow from Lemma 2.2, we obtain

$$\Big(\frac{1}{2}|\mathbf{u}_h|^2+F'(\rho_h)+\frac{1}{2}\kappa'(\rho_h)|\mathbf{q}_h|^2,(\rho_h)_t\Big)+(\rho_h\mathbf{u}_h,(\mathbf{u}_h)_t)+(\kappa(\rho_h)\mathbf{q}_h,(\mathbf{q}_h)_t)=0,$$

which gives (3.5). □

5 Time discretization

In this section, the semi-discrete LDG discretizations discussed in Sections 3 and 4 are extended to fully discrete schemes. We first discretize the GEK-C and IEK-C schemes in time using a first-order semi-implicit method. Next, we use these results to apply semi-implicit SDC time marching methods to achieve uniform higher-order accuracy, both in space and time.

5.1 First order time discretization

For the discretization in time, we first divide the time interval $[0,T]$ into M intervals using the partition $0=t^0<t^1<\cdots<t^n<\cdots<t^M=T$ and denote by $\Delta t^n=t^{n+1}-t^n$ the time step at time level n. We obtain two semi-implicit schemes with first order accuracy in time by linearizing the nonlinear high-order and first order terms in the EK-equations (3.1) and (1.3), respectively, as follows

$$\frac{\rho^{n+1}-\rho^n}{\Delta t^n}+\nabla\cdot(\rho^{n+1}\mathbf{u}^{n+1})=0, \tag{5.1a}$$

$$\begin{aligned}\frac{\rho^{n+1}\mathbf{u}^{n+1}-\rho^n\mathbf{u}^n}{\Delta t^n}&+\nabla\cdot(\rho^n\mathbf{u}^n\otimes\mathbf{u}^n)+\rho^n\nabla\Big(F'(\rho^n)-\kappa(\rho^n)\Delta\rho^{n+1}\\&-\frac{1}{2}\kappa'(\rho^n)\nabla\rho^n\cdot\nabla\rho^{n+1}\Big)=0,\end{aligned} \tag{5.1b}$$

and

$$\frac{\rho^{n+1}-\rho^n}{\Delta t^n}+\nabla\cdot(\rho^n\mathbf{u}^{n+1})=0, \tag{5.2a}$$

$$\frac{\mathbf{u}^{n+1}-\mathbf{u}^n}{\Delta t^n}+\nabla\left(\frac{1}{2}|\mathbf{u}^n|^2+F'(\rho^n)-\kappa(\rho^n)\Delta\rho^{n+1}-\frac{1}{2}\kappa'(\rho^n)\nabla\rho^n\cdot\nabla\rho^{n+1}\right)=0. \tag{5.2b}$$

By applying the LDG discretizations introduced in Section 3 and Section 4, the fully discrete schemes with first order accuracy in time can be summarized as follows:

- First order accurate time discretization for the GEK-C scheme

$$\left(\frac{\rho_h^{n+1}-\rho_h^n}{\Delta t^n},\phi\right)+\mathcal{D}^2(\rho_h^{n+1}\mathbf{u}_h^{n+1},\phi;\widehat{\rho_h^{n+1}\mathbf{u}_h^{n+1}})=0, \tag{5.3a}$$

$$\left(\frac{\mathbf{m}_h^{n+1}-\mathbf{m}_h^n}{\Delta t^n},\boldsymbol{\psi}\right)+\mathcal{D}^4(\rho_h^n\mathbf{u}_h^n\otimes\mathbf{u}_h^n,\boldsymbol{\psi};\widehat{\rho_h^n\mathbf{u}_h^n\otimes\mathbf{u}_h^n})$$
$$-\mathcal{D}^2\left(\rho_h^n\boldsymbol{\psi},f_h^n-r_h^{n+1}+s_h^{n+1}+\frac{1}{2}|\mathbf{u}_h^n|^2;\widehat{\rho_h^n\boldsymbol{\psi}}\right)=0, \tag{5.3b}$$

$$(r_h^{n+1},\theta)-\mathcal{D}^2(\mathbf{w}_h^{n+1},\theta;\widehat{\mathbf{w}_h^{n+1}})=0, \tag{5.3c}$$

$$(\mathbf{q}_h^n,\boldsymbol{\xi}_1)-\mathcal{D}^1(\rho_h^n,\boldsymbol{\xi}_1;\widehat{\rho_h^n})=0, \tag{5.3d}$$

$$(\mathbf{q}_h^{n+1},\boldsymbol{\xi}_2)-\mathcal{D}^1(\rho_h^{n+1},\boldsymbol{\xi}_2;\widehat{\rho_h^{n+1}})=0, \tag{5.3e}$$

$$(\rho_h^n\mathbf{u}_h^n,\boldsymbol{\eta}_1)-(\mathbf{m}_h^n,\boldsymbol{\eta}_1)=0, \tag{5.3f}$$

$$(\rho_h^{n+1}\mathbf{u}_h^{n+1},\boldsymbol{\eta}_2)-(\mathbf{m}_h^{n+1},\boldsymbol{\eta}_2)=0, \tag{5.3g}$$

$$(f_h^n,\zeta)-\left(F'(\rho_h^n)-\frac{1}{2}|\mathbf{u}_h^n|^2,\zeta\right)=0, \tag{5.3h}$$

$$(s_h^{n+1},\mu)-\frac{1}{2}(\kappa'(\rho_h^n)\mathbf{q}_h^n\cdot\mathbf{q}_h^{n+1},\mu)=0, \tag{5.3i}$$

$$(\mathbf{w}_h^{n+1},\boldsymbol{\nu})-(\kappa(\rho_h^n)\mathbf{q}_h^{n+1},\boldsymbol{\nu})=0, \tag{5.3j}$$

- First order accurate time discretization for the IEK-C scheme

$$\left(\frac{\rho_h^{n+1}-\rho_h^n}{\Delta t^n},\phi\right)+\mathcal{D}^2(\mathbf{m}_h^{n+1},\phi;\widehat{\mathbf{m}_h^{n+1}})=0, \tag{5.4a}$$

$$\left(\frac{\mathbf{u}_h^{n+1}-\mathbf{u}_h^n}{\Delta t^n},\boldsymbol{\psi}\right)+\mathcal{D}^1(f_h^n-r_h^{n+1}+s_h^{n+1},\boldsymbol{\psi};f_h^n-\widehat{r_h^{n+1}}+s_h^{n+1})=0, \tag{5.4b}$$

$$(r_h^{n+1},\theta)-\mathcal{D}^2(\mathbf{w}_h^{n+1},\theta;\widehat{\mathbf{w}_h^{n+1}})=0, \tag{5.4c}$$

$$(\mathbf{q}_h^n,\boldsymbol{\xi}_1)-\mathcal{D}^1(\rho_h^n,\boldsymbol{\xi}_1;\widehat{\rho_h^n})=0, \tag{5.4d}$$

$$(\mathbf{q}_h^{n+1},\boldsymbol{\xi}_2)-\mathcal{D}^1(\rho_h^{n+1},\boldsymbol{\xi}_2;\widehat{\rho_h^{n+1}})=0, \tag{5.4e}$$

$$(\mathbf{m}_h^{n+1},\boldsymbol{\eta})-(\rho_h^n\mathbf{u}_h^{n+1},\boldsymbol{\eta})=0, \tag{5.4f}$$

$$(f_h^n,\zeta)-\left(\frac{1}{2}|\mathbf{u}_h^n|^2+F'(\rho_h^n),\zeta\right)=0, \tag{5.4g}$$

$$(s_h^{n+1},\mu)-\frac{1}{2}(\kappa'(\rho_h^n)\mathbf{q}_h^n\cdot\mathbf{q}_h^{n+1},\mu)=0, \tag{5.4h}$$

$$(\mathbf{w}_h^{n+1},\boldsymbol{\nu})-(\kappa(\rho_h^n)\mathbf{q}_h^{n+1},\boldsymbol{\nu})=0. \tag{5.4i}$$

Note that the first order time discretization of the IEK-C scheme (5.4) will generate a linear system with respect to the degrees of freedom of ρ_h^{n+1} and $\mathbf{u}_h^{n+1}$. Although it is inevitable to use a Newton method for the solution of the nonlinear system (5.3), the linearization of the terms with high order spatial derivatives simplifies the Newton method considerably.

Next, we give details about the implementation of the two fully discrete schemes (5.3) and (5.4) with first-order accuracy in time. Given the solutions ρ_h^n and $\mathbf{m}_h^n$ at time level t^n, then the steps to update ρ_h^{n+1} and $\mathbf{m}_h^{n+1}$ in the GEK-C scheme (5.3) are as follows:

1). Based on (5.3f), compute $\mathbf{u}_h^n$ by solving a linear system whose matrix is associated with ρ_h^n.

2). From (5.3d) and (5.3h), compute $\mathbf{q}_h^n$ and f_h^n directly.

3). From (5.3e), (5.3i), (5.3j) and (5.3c), we know that s_h^{n+1} and r_h^{n+1} are linear functions in the unknown ρ_h^{n+1}, and from (5.3g), $\mathbf{u}_h^{n+1}$ is a function of $\mathbf{m}_h^{n+1}$. Then we can update ρ_h^{n+1} and $\mathbf{m}_h^{n+1}$ by substituting $s_h^{n+1}(\rho_h^{n+1})$, $r_h^{n+1}(\rho_h^{n+1})$ and $\mathbf{u}_h^{n+1}(\mathbf{m}_h^{n+1})$ into (5.3a) and (5.3b), which gives a nonlinear system with respect to ρ_h^{n+1} and $\mathbf{m}_h^{n+1}$.

Given the solutions ρ_h^n and $\mathbf{u}_h^n$ at time level t^n, then the steps to update ρ_h^{n+1} and $\mathbf{u}_h^{n+1}$ in the IEK-C scheme (5.4) are as follows:

1). From (5.4d) and (5.4g), compute $\mathbf{q}_h^n$ and f_h^n directly.

2). From (5.4e), (5.4h), (5.4i) and (5.4c), we know that s_h^{n+1} and r_h^{n+1} are linear functions in the unknown ρ_h^{n+1}, and from (5.4f), $\mathbf{m}_h^{n+1}$ is a linear function of $\mathbf{u}_h^{n+1}$. Then we can update ρ_h^{n+1} and $\mathbf{u}_h^{n+1}$ by substituting $s_h^{n+1}(\rho_h^{n+1})$, $r_h^{n+1}(\rho_h^{n+1})$ and $\mathbf{m}_h^{n+1}(\mathbf{u}_h^{n+1})$ into (5.4a) and (5.4b), and solve a linear system.

5.2 Semi-implicit SDC method

The semi-implicit SDC method is based on low-order time integration methods combined with iterative error reduction steps. The order of accuracy is increased with each additional iteration. The remarkable advantage of this method is that it is a one-step method, can be developed simply and systematically for any order of accuracy, and can handle ODEs without separating stiff and non-stiff terms [28].

To define the semi-implicit SDC scheme, we subdivide the time interval $[t^n,t^{n+1}]$ into P subintervals using the points $t^{n,m}$ for $m=0,1,\cdots,P$ such that $t^n=t^{n,0}<t^{n,1}<\cdots<t^{n,m}<$

$\cdots < t^{n,P} = t^{n+1}$. For convenience, we write the fully discrete schemes (5.3) and (5.4) with first-order time discretization as

$$\mathbf{U}^{n+1} = \mathbf{U}^n + \Delta t^n \mathbf{F}(t^n, \mathbf{U}^n, \mathbf{U}^{n+1}). \tag{5.5}$$

Let $\Delta t^{n,m} = t^{n,m+1} - t^{n,m}$ and $\mathbf{U}_k^{n,m}$ denote the k-th order approximation to $\mathbf{U}(t^{n,m})$. To avoid the instability caused by equispaced nodes in a high-order accurate discretization, the points $\{t^{n,m}\}_{m=0}^{p}$ are chosen to be the Gauss-Lobatto nodes on $[t^n, t^{n+1}]$. Then, the algorithm to calculate $\min(K+1, P+1)$-th order accurate numerical solutions of the EK-equations at time t^{n+1} is given in Algorithm 5.1. Here, K is the order of the polynomial basis functions and P is the number of Gauss-Lobatto points.

In Algorithm 5.1, $I_m^{m+1}(\mathbf{F}(t, \mathbf{U}_k, \mathbf{U}_k))$ is the integral of the P-th degree interpolating polynomial on the $P+1$ Gauss-Lobatto points $(t^{n,m}, \mathbf{F}(t^{n,m}, \mathbf{U}_k^{n,m}, \mathbf{U}_k^{n,m}))_{m=0}^{P}$ over the subinterval $[t^{n,m}, t^{n,m+1}]$, which is the numerical quadrature approximation of

$$\int_{t^{n,m}}^{t^{n,m+1}} \mathbf{F}(\tau, \mathbf{U}(\tau), \mathbf{U}(\tau)) d\tau.$$

In detail, to compute $I_m^{m+1}(\mathbf{F}(t, \mathbf{U}_k, \mathbf{U}_k))$, we first approximate $\mathbf{F}(t, \mathbf{U}_k, \mathbf{U}_k)$ by its Lagrange interpolation polynomial

$$\mathbf{F}_p(t, \mathbf{U}_k, \mathbf{U}_k) = \sum_{j=0}^{P} \mathbf{F}(t^{n,j}, \mathbf{U}_k^{n,j}, \mathbf{U}_k^{n,j}) \mathcal{L}_j^P(t),$$

using the Gauss-Lobatto points, with $\mathcal{L}_j^P(t)$ the j-th Lagrange interpolation function. Then

$$I_m^{m+1}(\mathbf{F}(t, \mathbf{U}_k, \mathbf{U}_k)) = \int_{t^{n,m}}^{t^{n,m+1}} \mathbf{F}_p(t, \mathbf{U}_k, \mathbf{U}_k) dt = \sum_{j=0}^{P} \mathbf{F}(t^{n,j}, \mathbf{U}_k^{n,j}, \mathbf{U}_k^{n,j}) \int_{t^{n,m}}^{t^{n,m+1}} \mathcal{L}_j^P(t).$$

The term $\theta \Delta t^{n,m} (\mathbf{F}(t^{n,m+1}, \mathbf{U}_k^{n,m+1}, \mathbf{U}_{k+1}^{n,m+1}) - \mathbf{F}(t^{n,m+1}, \mathbf{U}_k^{n,m+1}, \mathbf{U}_k^{n,m+1}))$ with $0 \le \theta \le 1$ in Algorithm 5.1, as demonstrated in [28], is helpful to the stability of the scheme, but it does not improve accuracy, whereas the term $I_m^{m+1}(\mathbf{F}(t, \mathbf{U}_k, \mathbf{U}_k))$ is responsible for the accuracy improvement. Usually, we take $K = P$ for efficiency reasons since the order of accuracy is bounded by $P+1$.

6 Numerical experiments

In this section, we will provide several numerical experiments for the EK-equations to illustrate the accuracy and capability of the proposed two LDG discretizations in conjunction with the semi-implicit SDC methods. We use rectangular meshes for the 2D

Algorithm 5.1 The semi-implicit SDC method.

Compute the initial first-order approximation

$\mathbf{U}_1^{n,0}=\mathbf{U}^n$
for $m=0,\cdots,P-1$ **do**
$\mathbf{U}_1^{n,m+1}=\mathbf{U}_1^{n,m}+\Delta t^{n,m}\mathbf{F}(t^{n,m},\mathbf{U}_1^{n,m},\mathbf{U}_1^{n,m+1})$
end for

Compute successive corrections

for $k=1,\cdots,K$ **do**
$\mathbf{U}_{k+1}^{n,0}=\mathbf{U}^n$
for $m=0,\cdots,P-1$ **do**

$$\mathbf{U}_{k+1}^{n,m+1}=\mathbf{U}_{k+1}^{n,m}+\theta\Delta t^{n,m}(\mathbf{F}(t^{n,m+1},\mathbf{U}_k^{n,m+1},\mathbf{U}_{k+1}^{n,m+1})-\mathbf{F}(t^{n,m+1},\mathbf{U}_k^{n,m+1},\mathbf{U}_k^{n,m+1}))+I_m^{m+1}(\mathbf{F}(t,\mathbf{U}_k,\mathbf{U}_k))$$

end for
end for
Finally we have $\mathbf{U}^{n+1}=\mathbf{U}_{K+1}^{n,P}$.

numerical examples. In all numerical experiments, unless otherwise stated, the $(k+1)$-th order SDC method will be utilized as a time discretization method when P^k (or Q^k) polynomials are employed. The time step Δt^n at time t^n is chosen to satisfy

$$\frac{d\Delta t^n}{\min_{K\in\mathcal{T}_h}h_K}\max_{K\in\mathcal{T}_h}|\bar{\mathbf{u}}_K\cdot\mathbf{n}_K\pm\sqrt{p'(\bar{\rho}_K)}|<CFL,$$

where $\bar{\rho}_K$ and $\bar{\mathbf{u}}_K$ represent the mean value of the density and velocity at element K, respectively, and CFL is the CFL number taken as 0.3, 0.18, 0.14, 0.1 for $k=1,2,3,4$, respectively. Note at every stage of the evolution in time, we solve the corresponding linear algebraic equations either with a direct solver (small problems) or the GMRES solver with ILU(0) or ILUC preconditioner (large problems).

6.1 Numerical results in 1D

Example 6.1 (One-dimensional EK-equations with van der Waals equation of state)**.** In order to demonstrate the high order accuracy, both in space and time, of the two LDG discretizations coupled with the semi-implicit SDC method, we choose a smooth exact solution for the one-dimensional EK-equations

$$\rho(x,t)=0.4+0.25e^{-t}\sin(x), \tag{6.1a}$$
$$u(x,t)=e^{-t}\cos(x), \tag{6.1b}$$

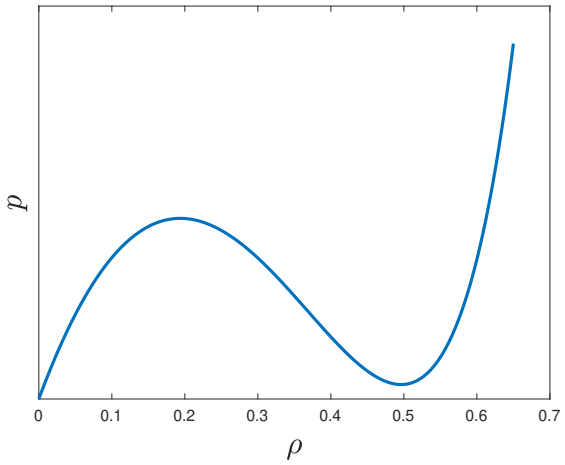

Figure 1: Example 6.1. The shape of the van der Waals pressure function $p=p(\rho)$ with $\theta=0.85$, $R=\frac{8}{27}$, $a=b=1$.

where an additional source term is added to the EK-equations to ensure that (6.1) is the exact solution. The EK-equations are closed using the van der Waals equation of state (1.5), which corresponds to a free energy density

$$F=R\theta\rho\log\frac{\rho}{b-\rho}-a\rho^2. \tag{6.2}$$

We take $\theta=0.85$, $R=\frac{8}{27}$, $a=b=1$, and use the domain $[0,2\pi]$ with periodic boundary conditions. The final simulation time is $T=0.1$. With these parameters we can plot the pressure p with respect to the density ρ in Fig. 1. It shows that the density defined in Eq. (6.1) has values in both liquid and vapor phases as well as in the spinodal region since $\rho\in[0.15,0.65]$.

Four different combinations of capillarity coefficients and stability parameters α_1 and α_2 are chosen. The corresponding L^2 errors and orders of the accuracy of the density and velocity computed with the GEK-C and IEK-C schemes are, respectively, shown for

- $\kappa=0.01$, $\alpha_1=0$, $\alpha_2=0$ (central fluxes), see Table 1,
- $\kappa=0.01$, $\alpha_1=-0.5$, $\alpha_2=-0.5$ (alternating fluxes), see Table 1,
- $\kappa=\frac{1}{4\rho}$, $\alpha_1=0$, $\alpha_2=0$ (central fluxes), see Table 2,
- $\kappa=\frac{1}{4\rho}$, $\alpha_1=-0.5$, $\alpha_2=-0.5$ (alternating fluxes), see Table 2.

It can be seen from these tables that the two energy conservative schemes, namely GEK-C and IEK-C, have optimal order of accuracy when *alternating numerical fluxes* ($\alpha_1=-0.5$, $\alpha_2=-0.5$) are used, but they exhibit accuracy degeneration in both the density ρ and

Table 1: Example 6.1. One-dimensional EK-equations with van der Waals equation of state and constant capillarity coefficient $\kappa=0.01$.

	N	GEK-C								IEK-C							
		$\alpha_1=0$, $\alpha_2=0$				$\alpha_1=-0.5$, $\alpha_2=-0.5$				$\alpha_1=0$, $\alpha_2=0$				$\alpha_1=-0.5$, $\alpha_2=-0.5$			
		$\|e_\rho\|_{L^2}$	Order	$\|e_u\|_{L^2}$	Order	$\|e_\rho\|_{L^2}$	Order	$\|e_u\|_{L^2}$	Order	$\|e_\rho\|_{L^2}$	Order	$\|e_u\|_{L^2}$	Order	$\|e_\rho\|_{L^2}$	Order	$\|e_u\|_{L^2}$	Order
P^1	16	8.98E-03	–	2.89E-02	–	1.04E-02	–	2.63E-02	–	9.77E-03	–	1.87E-02	–	8.83E-03	–	2.49E-02	–
	32	4.64E-03	0.95	1.35E-02	1.09	1.42E-03	2.87	5.96E-03	2.14	4.93E-03	0.98	9.10E-03	1.04	1.61E-03	2.45	7.51E-03	1.73
	64	2.33E-03	0.99	6.64E-03	1.02	2.40E-04	2.56	1.02E-03	2.53	2.47E-03	1.00	4.52E-03	1.00	2.48E-04	2.70	1.34E-03	2.48
	128	1.17E-03	1.00	3.30E-03	1.00	5.89E-05	2.03	2.47E-04	2.05	1.23E-03	1.00	2.25E-03	1.00	5.96E-05	2.06	3.26E-04	2.03
P^2	16	1.34E-04	–	7.00E-04	–	2.31E-04	–	1.02E-03	–	1.50E-04	–	5.61E-04	–	4.47E-04	–	1.46E-03	–
	32	9.68E-06	3.79	8.53E-05	3.04	1.57E-05	3.88	1.27E-04	3.01	9.69E-06	3.95	4.38E-05	3.67	5.72E-05	2.96	3.09E-04	2.24
	64	1.20E-06	3.00	1.06E-05	3.00	1.87E-06	3.06	1.21E-05	3.38	1.19E-06	3.01	4.89E-06	3.16	2.13E-06	4.74	1.81E-05	4.09
	128	1.50E-07	3.00	1.33E-06	3.00	2.32E-07	3.01	1.50E-06	3.00	1.49E-07	3.00	6.01E-07	3.02	2.37E-07	3.16	2.14E-06	3.07
P^3	16	3.43E-05	–	8.28E-05	–	1.00E-05	–	4.57E-05	–	2.89E-05	–	1.82E-04	–	1.25E-05	–	7.29E-05	–
	32	4.69E-06	2.87	1.01E-05	3.03	2.90E-07	5.11	2.67E-06	4.09	3.14E-06	3.20	1.99E-05	3.19	6.45E-07	4.28	4.55E-06	4.00
	64	6.21E-07	2.92	1.26E-06	3.00	1.24E-08	4.54	1.57E-07	4.08	3.98E-07	2.98	2.74E-06	2.86	1.58E-08	5.34	2.46E-07	4.20
	128	7.86E-08	2.98	1.57E-07	3.00	7.01E-10	4.14	9.50E-09	4.04	5.02E-08	2.99	3.49E-07	2.97	7.10E-10	4.47	1.22E-08	4.33
P^4	16	2.24E-07	–	1.81E-06	–	3.28E-07	–	1.85E-06	–	2.43E-07	–	1.28E-06	–	4.73E-07	–	3.34E-06	–
	32	1.25E-09	7.48	5.26E-08	5.11	3.32E-09	6.62	5.53E-08	5.06	1.41E-09	7.42	1.21E-08	6.71	5.40E-09	6.45	9.85E-08	5.08
	64	3.66E-11	5.09	1.64E-09	5.00	5.72E-11	5.86	1.65E-09	5.06	3.66E-11	5.27	2.14E-10	5.82	7.53E-11	6.16	2.00E-09	5.61
	128	1.14E-12	5.00	5.14E-11	5.00	1.70E-12	5.06	5.16E-11	5.00	1.13E-12	5.00	5.13E-12	5.38	1.76E-12	5.41	6.01E-11	5.06

Table 2: Example 6.1. One-dimensional EK-equations with van der Waals equation of state and capillarity coefficient $\kappa=\frac{1}{4\rho}$.

	N	GEK-C								IEK-C							
		$\alpha_1=0$, $\alpha_2=0$				$\alpha_1=-0.5$, $\alpha_2=-0.5$				$\alpha_1=0$, $\alpha_2=0$				$\alpha_1=-0.5$, $\alpha_2=-0.5$			
		$\|e_\rho\|_{L^2}$	Order	$\|e_u\|_{L^2}$	Order	$\|e_\rho\|_{L^2}$	Order	$\|e_u\|_{L^2}$	Order	$\|e_\rho\|_{L^2}$	Order	$\|e_u\|_{L^2}$	Order	$\|e_\rho\|_{L^2}$	Order	$\|e_u\|_{L^2}$	Order
P^1	16	8.91E-03	–	4.66E-02	–	4.23E-03	–	3.89E-02	–	8.29E-03	–	6.65E-02	–	4.39E-03	–	4.39E-02	–
	32	4.36E-03	1.03	2.37E-02	0.97	9.88E-04	2.09	6.51E-03	2.57	4.04E-03	1.03	3.77E-02	0.81	9.95E-04	2.14	7.71E-03	2.51
	64	2.18E-03	1.00	1.19E-02	0.99	2.40E-04	2.04	1.10E-03	2.55	2.03E-03	0.99	1.96E-02	0.94	2.40E-04	2.04	1.33E-03	2.52
	128	1.09E-03	1.00	5.98E-03	1.00	5.90E-05	2.02	2.60E-04	2.08	1.02E-03	0.99	9.88E-03	0.99	5.91E-05	2.02	3.24E-04	2.04
P^2	16	8.39E-05	–	7.62E-04	–	1.36E-04	–	8.52E-04	–	8.51E-05	–	6.90E-04	–	1.08E-04	–	9.65E-04	–
	32	9.68E-06	3.11	8.56E-05	3.15	1.48E-05	3.19	9.92E-05	3.10	9.63E-06	3.14	4.25E-05	4.02	1.46E-05	2.89	1.36E-04	2.82
	64	1.20E-06	3.00	1.06E-05	3.00	1.86E-06	3.00	1.20E-05	3.03	1.20E-06	3.00	4.91E-06	3.11	1.85E-06	2.98	1.69E-05	3.00
	128	1.51E-07	3.00	1.33E-06	3.00	2.32E-07	3.00	1.51E-06	3.00	1.49E-07	3.00	6.04E-07	3.02	2.31E-07	3.00	2.11E-06	3.00
P^3	16	2.36E-05	–	1.02E-04	–	3.04E-06	–	4.65E-05	–	1.74E-05	–	1.00E-04	–	3.24E-06	–	5.71E-05	–
	32	3.10E-06	2.92	1.35E-05	2.92	1.79E-07	4.08	2.45E-06	4.24	2.37E-06	2.88	2.56E-05	1.96	1.81E-07	4.16	3.18E-06	4.16
	64	3.89E-07	3.00	1.77E-06	2.93	1.12E-08	4.00	1.52E-07	4.01	2.95E-07	3.00	3.06E-06	3.06	1.12E-08	4.01	1.94E-07	4.03
	128	4.86E-08	3.00	2.24E-07	2.98	7.01E-10	4.00	9.52E-09	4.00	3.71E-08	3.00	3.71E-07	3.04	6.99E-10	4.00	1.21E-08	4.00
P^4	16	5.24E-07	–	9.21E-06	–	6.80E-08	–	1.81E-06	–	6.77E-07	–	1.24E-05	–	7.19E-08	–	2.30E-06	–
	32	1.22E-09	8.74	5.29E-08	7.44	1.84E-09	5.20	5.30E-08	5.10	1.22E-09	9.10	1.35E-08	9.84	1.86E-09	5.26	6.15E-08	5.22
	64	3.67E-11	5.05	1.64E-09	5.00	5.53E-11	5.05	1.65E-09	5.00	3.65E-11	5.07	2.09E-10	6.01	5.53E-11	5.07	1.89E-09	5.01
	128	1.15E-12	5.00	5.14E-11	5.00	1.73E-12	5.00	5.18E-11	5.00	1.14E-12	5.00	5.22E-12	5.32	1.73E-12	4.99	5.96E-11	4.99

velocity u when central fluxes and odd degree polynomial basis functions are adopted. We point out that the results with alternating numerical fluxes for the other three cases $\alpha_1=-0.5$, $\alpha_2=0.5$, and $\alpha_1=0.5$, $\alpha_2=-0.5$, and $\alpha_1=0.5$ $\alpha_2=0.5$ are nearly identical to the case $\alpha_1=-0.5$, $\alpha_2=-0.5$, and will not be displayed. For the remaining test cases, we will therefore only show results for the GEK-C and IEK-C schemes with alternating fluxes ($\alpha_1=-0.5$, $\alpha_2=-0.5$), which schemes will achieve optimal convergence rates for smooth solutions.

The main properties of the two LDG discretizations, namely the GEK-C and IEK-C, are summarized in Table 3.

Example 6.2 (Periodic wave solutions of the QHD equations corresponding to the cubic NLS equation)**.** Next, the application of our methods to QHD fields will be investigated. We consider $\epsilon=1$, $g(\rho)=\beta\rho$ in the QHD equations (4.5) in 1D, which correspond to the NLS equation (4.1) with a cubic nonlinearity $\beta|\psi|^2$. The two kinds of periodic wave

Table 3: Summary of properties of the GEK-C and IEK-C schemes.

	GEK-C	IEK-C
Equation solved	Eq. (3.1)	Eq. (1.3) with $\nabla\times\mathbf{u}=\mathbf{0}$
Energy bound	Conservative	Conservative
Convergence (alternating fluxes)	Optimal	Optimal
Convergence (central fluxes)	Suboptimal (ρ,$\mathbf{u}$) for odd polynomials, otherwise optimal	Suboptimal (ρ,$\mathbf{u}$) for odd polynomials, otherwise optimal

solutions of the QHD equations (4.5) for the above parameters are [27]:

- first kind periodic wave solution

$$\rho(x,t)=\rho_1-(\rho_1-\rho_3)\mathrm{dn}^2(\omega(x-v_0t),m), \tag{6.3a}$$
$$u(x,t)=v_0+\frac{c_1}{\rho(x,t)}, \tag{6.3b}$$

  with $\omega=\sqrt{\beta(\rho_1-\rho_3)}$, $\beta>0$, $\rho_1>\rho_2>\rho_3>0$, $m=\frac{\rho_2-\rho_3}{\rho_1-\rho_3}$,

- second kind periodic wave solution

$$\rho(x,t)=\rho_3+(\rho_1-\rho_3)\mathrm{dn}^2(\omega(x-v_0t),m), \tag{6.4a}$$
$$u(x,t)=v_0+\frac{c_1}{\rho(x,t)}, \tag{6.4b}$$

  with $\omega=\sqrt{-\beta(\rho_1-\rho_3)}$, $\beta<0$, $\rho_1>\rho_2>0>\rho_3$, $|\rho_3|>\rho_1+\rho_2$, $m=\frac{\rho_1-\rho_2}{\rho_1-\rho_3}$,

where $\mathrm{dn}(\cdot,m)$ is the delta amplitude function with elliptic modulus m [32], and

$$v_0^2=\beta(\rho_1+\rho_2+\rho_3),\quad c_1^2=\beta\rho_1\rho_2\rho_3.$$

The period of these two periodic wave solutions is $T_p=2K(m)/\omega$, with $K(m)$ the complete elliptic integral of the first kind. We solve the QHD equations with periodic solutions (6.3) and (6.4), respectively, on the domain $[-T_p,T_p]$, till time $T=0.5$ using the LDG discretizations GEK-C and IEK-C. As shown in Tables 4 and 5, both schemes achieve optimal order of accuracy as long as suitable numerical fluxes are used.

Example 6.3 (Gray soliton solutions of the QHD equations corresponding to the cubic NLS equation)**.** Next, we study the gray soliton solutions

$$\rho(x,t)=\rho_3+(\rho_1-\rho_3)\tanh^2\left(\sqrt{\beta(\rho_1-\rho_3)}(x-v_0t)\right), \tag{6.5a}$$
$$u(x,t)=v_0+\frac{c_1}{\rho(x,t)}, \tag{6.5b}$$

Table 4: Example 6.2. Periodic wave solution (6.3) of the 1D QHD equations with $\beta=1$, $\rho_1=2$, $\rho_2=1.5$, $\rho_3=0.8$. $\alpha_1=-0.5$, $\alpha_2=-0.5$ (alternating fluxes).

	N	GEK-C				IEK-C			
		$\|e_\rho\|_{L^2}$	Order	$\|e_u\|_{L^2}$	Order	$\|e_\rho\|_{L^2}$	Order	$\|e_u\|_{L^2}$	Order
P^1	32	7.57E-03	–	1.39E-02	–	9.65E-03	–	3.94E-02	–
	64	1.77E-03	2.09	3.16E-03	2.13	2.12E-03	2.18	8.99E-03	2.13
	128	4.35E-04	2.03	7.75E-04	2.02	5.18E-04	2.03	2.20E-03	2.02
	256	1.08E-04	2.01	1.93E-04	2.00	1.28E-04	2.00	5.48E-04	2.00
P^2	32	2.66E-04	–	6.67E-04	–	2.84E-04	–	1.37E-03	–
	64	3.27E-05	3.02	7.96E-05	3.06	3.36E-05	3.07	1.62E-04	3.07
	128	4.08E-06	3.00	9.88E-06	3.01	4.15E-06	3.01	2.00E-05	3.01
	256	5.10E-07	3.00	1.23E-06	3.00	5.18E-07	3.00	2.50E-06	3.00
P^3	32	1.18E-05	–	6.91E-05	–	1.13E-05	–	7.89E-05	–
	64	6.22E-07	4.25	2.38E-06	4.85	6.25E-07	4.17	3.68E-06	4.41
	128	3.88E-08	4.00	1.49E-07	4.00	3.89E-08	4.00	2.29E-07	4.00
	256	2.42E-09	4.00	9.32E-09	4.00	2.43E-09	4.00	1.43E-08	4.00
P^4	32	4.05E-07	–	2.82E-06	–	4.27E-07	–	3.77E-06	–
	64	1.21E-08	5.06	7.74E-08	5.18	1.21E-08	5.13	8.87E-08	5.41
	128	3.77E-10	5.00	2.33E-09	5.04	3.77E-10	5.00	2.73E-09	5.01
	200	4.05E-11	5.00	2.53E-10	4.98	4.05E-11	5.00	2.96E-10	4.98

Table 5: Example 6.2. Periodic wave solution (6.4) of the 1D QHD equations with $\beta=-1$, $\rho_1=0.3$, $\rho_2=0.1$, $\rho_3=-0.5$. $\alpha_1=-0.5$, $\alpha_2=-0.5$ (alternating fluxes).

	N	GEK-C				IEK-C			
		$\|e_\rho\|_{L^2}$	Order	$\|e_u\|_{L^2}$	Order	$\|e_\rho\|_{L^2}$	Order	$\|e_u\|_{L^2}$	Order
P^1	32	1.88E-03	–	1.17E-02	–	1.88E-03	–	1.71E-02	–
	64	4.64E-04	2.01	2.90E-03	2.01	4.65E-04	2.02	4.18E-03	2.03
	128	1.15E-04	2.00	7.23E-04	2.00	1.15E-04	2.00	1.04E-03	2.00
	256	2.89E-05	2.00	1.80E-04	2.00	2.89E-05	2.00	2.60E-04	2.00
P^2	32	6.01E-05	–	4.74E-04	–	6.03E-05	–	4.96E-04	–
	64	7.47E-06	3.00	5.99E-05	2.98	7.48E-06	3.01	6.14E-05	3.01
	128	9.32E-07	3.00	7.52E-06	2.99	9.33E-07	3.00	7.66E-06	3.00
	256	1.16E-07	3.00	9.40E-07	3.00	1.16E-07	3.00	9.57E-07	3.00
P^3	32	1.61E-06	–	2.78E-05	–	1.61E-06	–	2.64E-05	–
	64	1.00E-07	4.00	1.77E-06	3.97	1.00E-07	4.00	1.65E-06	4.00
	128	6.25E-09	4.00	1.11E-07	3.99	6.25E-09	4.00	1.03E-07	4.00
	256	3.90E-10	4.00	6.97E-09	4.00	3.90E-10	4.00	6.46E-09	4.00
P^4	32	4.20E-08	–	1.70E-06	–	4.21E-08	–	1.57E-06	–
	64	1.30E-09	5.01	5.48E-08	4.96	1.30E-09	5.01	5.00E-08	4.98
	128	4.05E-11	5.00	1.72E-09	4.99	4.05E-11	5.00	1.56E-09	5.00
	200	4.40E-12	4.98	1.86E-10	4.99	4.42E-12	4.96	1.70E-10	4.98

Table 6: Example 6.3. Gray soliton solution (6.5) of the 1D QHD equations with $\beta=1$, $\rho_1=1.5$, $\rho_3=1$, $v_0=2$. $\alpha_1=-0.5$, $\alpha_2=-0.5$ (alternating fluxes).

	N	GEK-C				IEK-C			
		$\|e_\rho\|_{L^2}$	Order	$\|e_u\|_{L^2}$	Order	$\|e_\rho\|_{L^2}$	Order	$\|e_u\|_{L^2}$	Order
P^1	200	1.53E-03	–	1.91E-03	–	1.76E-03	–	5.59E-03	–
	400	3.64E-04	2.07	4.55E-04	2.07	4.08E-04	2.11	1.34E-03	2.05
	800	8.97E-05	2.02	1.12E-04	2.01	9.97E-05	2.03	3.32E-04	2.01
	1600	2.23E-05	2.00	2.81E-05	2.00	2.47E-05	2.00	8.30E-05	2.00
P^2	200	3.52E-05	–	5.31E-05	–	3.57E-05	–	1.36E-04	–
	400	4.40E-06	3.00	6.51E-06	3.02	4.34E-06	3.04	1.65E-05	3.04
	800	5.51E-07	3.00	8.11E-07	3.00	5.39E-07	3.00	2.06E-06	3.00
	1600	6.88E-08	3.00	1.01E-07	3.00	6.72E-08	3.00	2.57E-07	3.00
P^3	200	8.93E-07	–	1.87E-06	–	8.98E-07	–	3.81E-06	–
	400	5.55E-08	4.00	1.02E-07	4.18	5.57E-08	4.01	2.26E-07	4.07
	800	3.47E-09	4.00	6.42E-09	4.00	3.47E-09	4.00	1.40E-08	4.00
	1600	2.16E-10	4.00	4.01E-10	4.00	2.17E-10	4.00	8.80E-10	4.00
P^4	100	7.42E-07	–	1.94E-06	–	8.33E-07	–	3.71E-06	–
	200	2.31E-08	5.00	7.18E-08	4.75	2.35E-08	5.14	1.14E-07	5.02
	400	7.11E-10	5.02	1.68E-09	5.41	7.12E-10	5.04	3.02E-09	5.24
	800	2.22E-11	5.00	5.31E-11	4.98	2.22E-11	5.00	9.49E-11	4.99

of the QHD equations (4.5) with $\epsilon=1$, $g(\rho)=\beta\rho$, $\beta>0$, where $\rho_1>\rho_3>0$, v_0 is an arbitrary value, $c_1=\pm\rho_1\sqrt{\beta\rho_3}$ [27]. A "local" traveling wave whose envelope has one global peak and decays far away from the peak is called a solitary wave. Solitons are those self-reinforcing solitary waves that retain their shape and velocity during wave propagation, even after interacting with other solitons, due to the exact balance between the nonlinear term and the wave packet dispersion. The gray solitons (6.5) with $\rho(0)=\rho_3$, $\rho(\infty)=\rho_1$, have a convex-shaped density with a non-trivial phase jump across the density minimum that can be supported in defocusing media. Owing to the exponential decay of the solitons (6.5) away from the crest, we conduct the simulations on the domain $[-20,20]$ with periodic boundary conditions. The computed results of the proposed LDG discretizations with alternating numerical fluxes at $T=1$ are presented in Table 6, which shows that both LDG discretizations have an optimal rate of convergence.

Example 6.4 (Shallow water equations with dispersive perturbations)**.** In this example, we will test the performance of the LDG discretization for shallow water waves. Specifically, we consider shallow water equations without friction at the bottom and with dispersive perturbations

$$\begin{aligned} &h_t+(hu)_x=0,\\ &(hu)_t+\left(hu^2+\frac{1}{2}gh^2\right)_x=\kappa hh_{xxx}. \end{aligned}$$

This system corresponds to the 1D EK-equations with ρ replaced by h, $p=\frac{1}{2}gh^2$, $F=\frac{1}{2}gh^2$,

and constant capillarity coefficient κ. We choose g=9.8, $\kappa=\frac{67}{1134000}$, and the initial solutions are

$$h(x,0)=10^{-3}(1+0.3e^{-2000(x-0.4)^2}),\quad u(x,0)=0.$$

The computational domain with periodic boundary conditions is $[0,0.8]$ and the final simulation time is $T=1$. The initial wave profile and profiles of the wave height computed with P^2 and P^4 elements at $t=1$ are shown in Fig. 2. We can see that both LDG discretizations correctly capture the capillary ripples, even using 400 cells, compared with the results in [42] using 3000 cells. The energy evolution of the two schemes during the simulation is presented in Fig. 3 clearly indicates that both schemes can conserve energy within a machine tolerance despite using a non-conservative SDC time discretization.

6.2 Numerical results in 2D

Example 6.5 (Two-dimensional EK-equations with van der Waals equation of state)**.** In this example, we extend the accuracy test for the EK-equations with a van der Waals equation of state to two dimensions. We construct the following smooth solutions

$$\begin{aligned}\rho(\mathbf{x},t)&=0.5+0.2e^{-t}\sin(x)\sin(y),\\ u(\mathbf{x},t)&=e^{-t}\sin(x)\cos(y),\\ v(\mathbf{x},t)&=e^{-t}\cos(x)\sin(y),\end{aligned}$$

with an irrotational velocity field, which satisfies the two-dimensional EK-equations with an appropriate source term. We choose $\theta=0.85$, $R=\frac{8}{27}$, $a=b=1$ in (1.5). The results computed on the domain $[0,2\pi]^2$ with periodic boundary conditions are presented in Table 7 for the constant capillarity coefficient $\kappa=0.01$. Suboptimal order of accuracy for the velocity $\mathbf{u}$ is observed for the GEK-C and IEK-C schemes with P^2 element in Tables 7. An implementation of Q^k element will remedy this, as shown in Table 8 for the constant capillarity coefficient $\kappa=0.01$, and in Table 9 for the variable capillarity coefficient $\kappa=\frac{1}{4\rho}$.

Example 6.6 (Singular solutions of the two-dimensional QHD equations)**.** In this test case, we investigate three singular solutions of the two-dimensional QHD equations (4.5) with $\epsilon=2$ and $g(\rho)=-\rho$. The three initial density functions are given by [45,52,59,60]

- Initial density I

$$\rho(\mathbf{x},0)=((1.1+\sin x)(2+\sin y))^2, \tag{6.6}$$

- Initial density II

$$\rho(\mathbf{x},0)=\left(2+0.01\sin\left(x+\frac{\pi}{4}\right)\sin\left(y+\frac{\pi}{4}\right)\right)^2, \tag{6.7}$$

- Initial density III

$$\rho(\mathbf{x},0)=\left(0.1+6\sqrt{2}e^{-x^2-y^2}\right)^2, \tag{6.8}$$

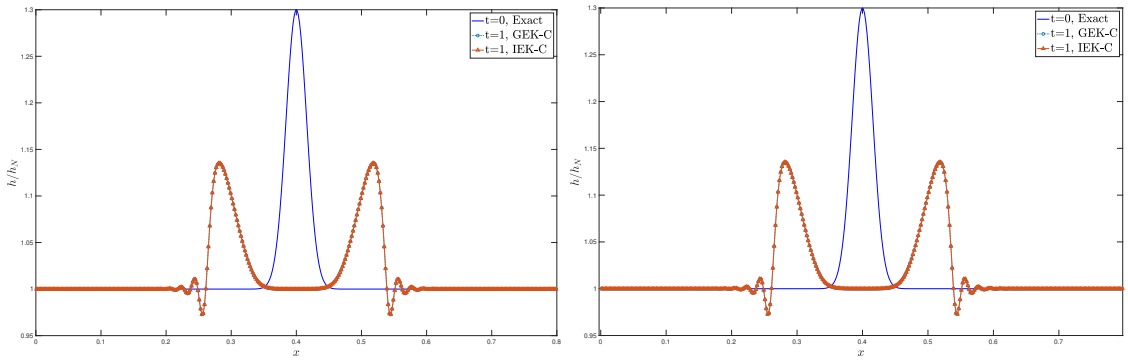

(a) P^2 (b) P^4

Figure 2: Example 6.4. Wave height at time $t=1$ for the shallow water equations with dispersive perturbations. P^2 and P^4 elements with 400 uniform cells.

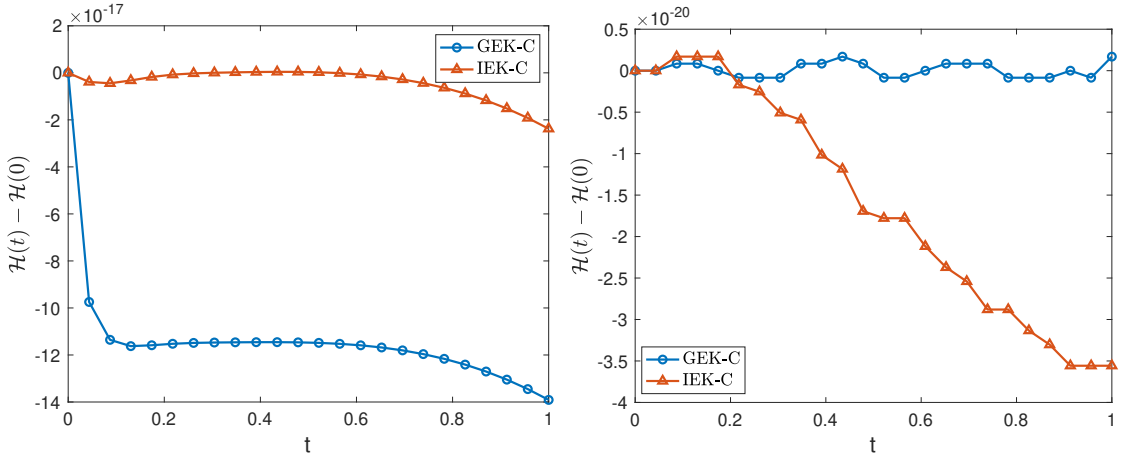

(a) P^2 (b) P^4

Figure 3: Example 6.4. Energy evolution for the shallow water equations with dispersive perturbations. P^2 and P^4 elements with 400 uniform cells.

respectively. Note, compared with the initial conditions in [45, 52, 59] for the NLS equation, the initial density functions (6.6) and (6.8) have been slightly modified to ensure the positivity of the computed density. The initial velocity field vanishes, i.e., $u(\mathbf{x},0)=v(\mathbf{x},0)=0$. We perform simulations for the initial conditions (6.6)-(6.8) with periodic boundary conditions on, respectively, the domains $[0,2\pi]^2$, $[-\pi,\pi]^2$ and $[-5,5]^2$.

In order to accurately and efficiently capture the singular solutions of the QHD equations when blow-up phenomena occur, an h-adaptive technique is employed. The gradient of the density is used to control the adaption. We first compute in each element

Table 7: Example 6.5. Two-dimensional EK-equations with van der Waals equation of state and constant capillarity coefficient $\kappa=0.01$. P^k basis functions. $\alpha_1=-0.5$, $\alpha_2=-0.5$ (alternating fluxes).

	N	GEK-C				IEK-C			
		$\|e_\rho\|_{L^2}$	Order	$\|e_u\|_{L^2}$	Order	$\|e_\rho\|_{L^2}$	Order	$\|e_u\|_{L^2}$	Order
P^1	10	6.24E-02	–	1.87E-01	–	4.74E-02	–	1.71E-01	–
	20	2.09E-02	1.57	7.02E-02	1.41	1.43E-02	1.72	5.80E-02	1.56
	40	2.31E-03	3.18	1.41E-02	2.31	1.75E-03	3.03	1.15E-02	2.33
	80	4.19E-04	2.46	3.61E-03	1.97	4.23E-04	2.04	2.83E-03	2.01
P^2	10	8.29E-03	–	2.74E-02	–	1.08E-02	–	3.03E-02	–
	20	7.59E-04	3.44	4.19E-03	2.71	1.02E-03	3.40	5.71E-03	2.40
	40	5.46E-05	3.79	8.13E-04	2.36	5.12E-05	4.32	1.12E-03	2.34
	80	5.34E-06	3.35	1.78E-04	2.19	5.51E-06	3.21	2.69E-04	2.05

Table 8: Example 6.5. Two-dimensional EK-equations with van der Waals equation of state and constant capillarity coefficient $\kappa=0.01$. Q^k basis functions. $\alpha_1=-0.5$, $\alpha_2=-0.5$ (alternating fluxes).

	N	GEK-C				IEK-C			
		$\|e_\rho\|_{L^2}$	Order	$\|e_u\|_{L^2}$	Order	$\|e_\rho\|_{L^2}$	Order	$\|e_u\|_{L^2}$	Order
P^1	10	6.47E-02	–	1.86E-01	–	4.36E-02	–	1.06E-01	–
	20	2.00E-02	1.69	6.96E-02	1.41	1.53E-02	1.50	5.07E-02	1.06
	40	1.69E-03	3.56	1.40E-02	2.31	1.37E-03	3.49	8.21E-03	2.62
	80	4.19E-04	2.01	3.61E-03	1.96	3.03E-04	2.17	1.83E-03	2.16
P^2	10	3.29E-03	–	8.97E-03	–	3.36E-03	–	8.41E-03	–
	20	4.82E-04	2.77	1.46E-03	2.61	4.26E-04	2.98	9.61E-04	3.12
	40	2.14E-05	4.49	1.34E-04	3.44	1.71E-05	4.63	1.28E-04	2.91
	80	1.95E-06	3.45	1.27E-05	3.40	1.91E-06	3.16	1.30E-05	3.29

Table 9: Example 6.5. Two-dimensional EK-equations with van der Waals equation of state and capillarity coefficient $\kappa=\frac{1}{4\rho}$. Q^k basis functions. $\alpha_1=-0.5$, $\alpha_2=-0.5$ (alternating fluxes).

	N	GEK-C				IEK-C			
		$\|e_\rho\|_{L^2}$	Order	$\|e_u\|_{L^2}$	Order	$\|e_\rho\|_{L^2}$	Order	$\|e_u\|_{L^2}$	Order
P^1	10	2.30E-02	–	1.13E-01	–	2.66E-02	–	1.49E-01	–
	20	4.98E-03	2.21	2.43E-02	2.22	4.93E-03	2.43	3.23E-02	2.20
	40	1.20E-03	2.04	6.26E-03	1.96	1.19E-03	2.03	7.22E-03	2.16
	80	3.01E-04	2.00	1.86E-03	1.75	3.02E-04	1.99	1.81E-03	1.99
P^2	10	1.48E-03	–	9.12E-03	–	9.68E-04	–	9.73E-03	–
	20	1.12E-04	3.72	7.67E-04	3.57	1.15E-04	3.06	8.39E-04	3.53
	40	1.52E-05	2.88	1.01E-04	2.92	1.51E-05	2.93	1.03E-04	3.01
	80	1.90E-06	3.00	1.26E-05	3.00	1.89E-06	3.00	1.35E-05	2.94

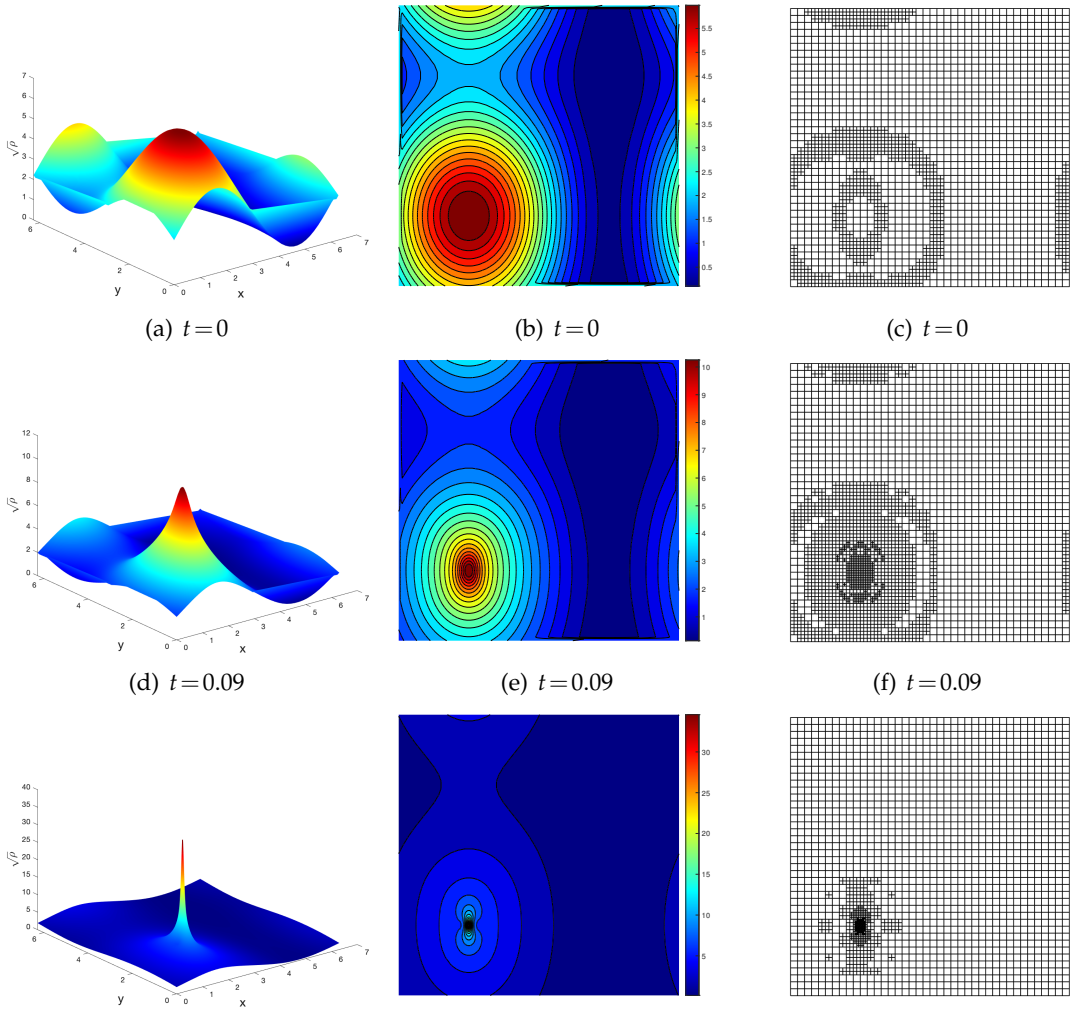

(a) $t=0$ (b) $t=0$ (c) $t=0$

(d) $t=0.09$ (e) $t=0.09$ (f) $t=0.09$

(g) $t=0.104$ (h) $t=0.104$ (i) $t=0.104$

Figure 4: Example 6.6. Blow up phenomenon for 2D QHD equations with initial density (6.6) computed with the IEK-C scheme. The square root of the density and corresponding adaptive mesh. Q^2 elements and initial mesh of 40×40 cells.

$K\in\mathcal{T}_h$

$$\eta_{gi}=|\nabla\rho|d_i^{\frac{3}{2}},\quad i=1,\cdots,N_c,$$

where N_c is the total number of elements and $d_i=\sqrt{|K|}$. The standard deviation of the gradient of density is then

$$\eta_g=\sqrt{\frac{\sum_{i=1}^{N_c}\eta_{gi}^2}{N_c}}.$$

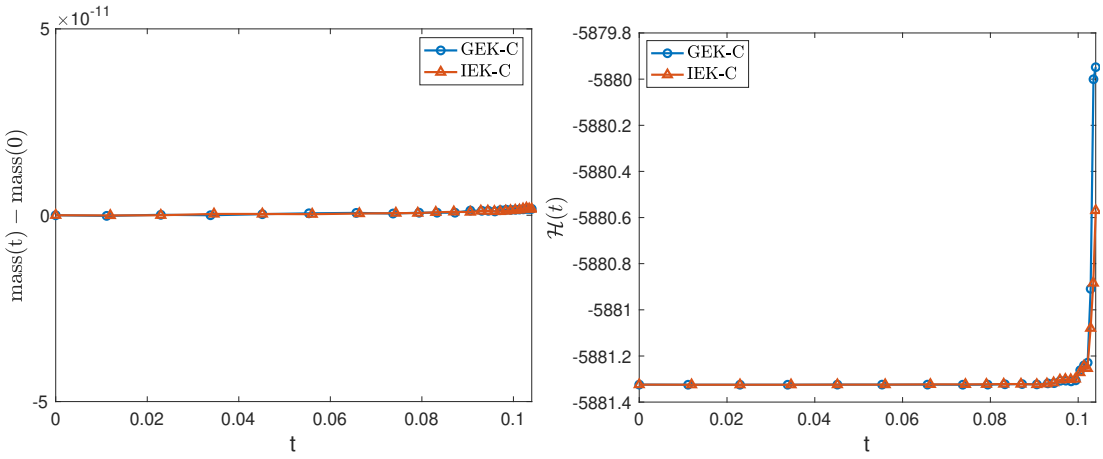

(a) Mass loss evolution (b) Energy evolution

Figure 5: Example 6.6. Blow up phenomenon for 2D QHD equations with initial density (6.6) computed with the IEK-C scheme. Mass loss and energy evolution. Q^2 elements and initial mesh of 40×40 cells.

Suppose that the mesh level of all elements in the initial mesh equals zero, and each element in the initial mesh can be refined at most LEV-times. Then

- if $\eta_{gi} > \omega_1 \eta_g$ and the level of $K < LEV$, then K is marked as a candidate element for refinement,

- if $\eta_{gi} < \omega_2 \eta_g$ and the level of $K > 0$, then K is marked as a candidate element for coarsening,

with ω_l, $l = 1,2$ problem dependent parameters. For more details on the adaption algorithm, see [36, 39]. In this example, we choose $\omega_1 = 1.7$, $\omega_2 = 0.7$. The square root of the density coupled with the corresponding adaptive mesh at different times, computed by the IEK-C scheme are shown in Figs. 4, 6 and 8. The results show that the solutions with sine initial density functions (6.6) and (6.7) will blow up in a finite time, with one peak in Fig. 4 and two peaks in Fig. 6. A much stronger singular solution with exponential initial density function (6.8) is observed in Fig. 8, with the maximum density increased by more than three thousand. Also, the IEK-C scheme captures this blow-up phenomenon accurately. The numerical results computed with the GEK-C scheme are nearly identical to those of the IEK-C scheme, and therefore will not be displayed. The mass loss and energy evolution for both LDG discretizations are shown in Figs. 5, 7 and 9. We observe that the computed mass remains within the machine tolerance, although the QHD equations contain singular solutions. The numerical energy increases when the solutions begin to blow up.

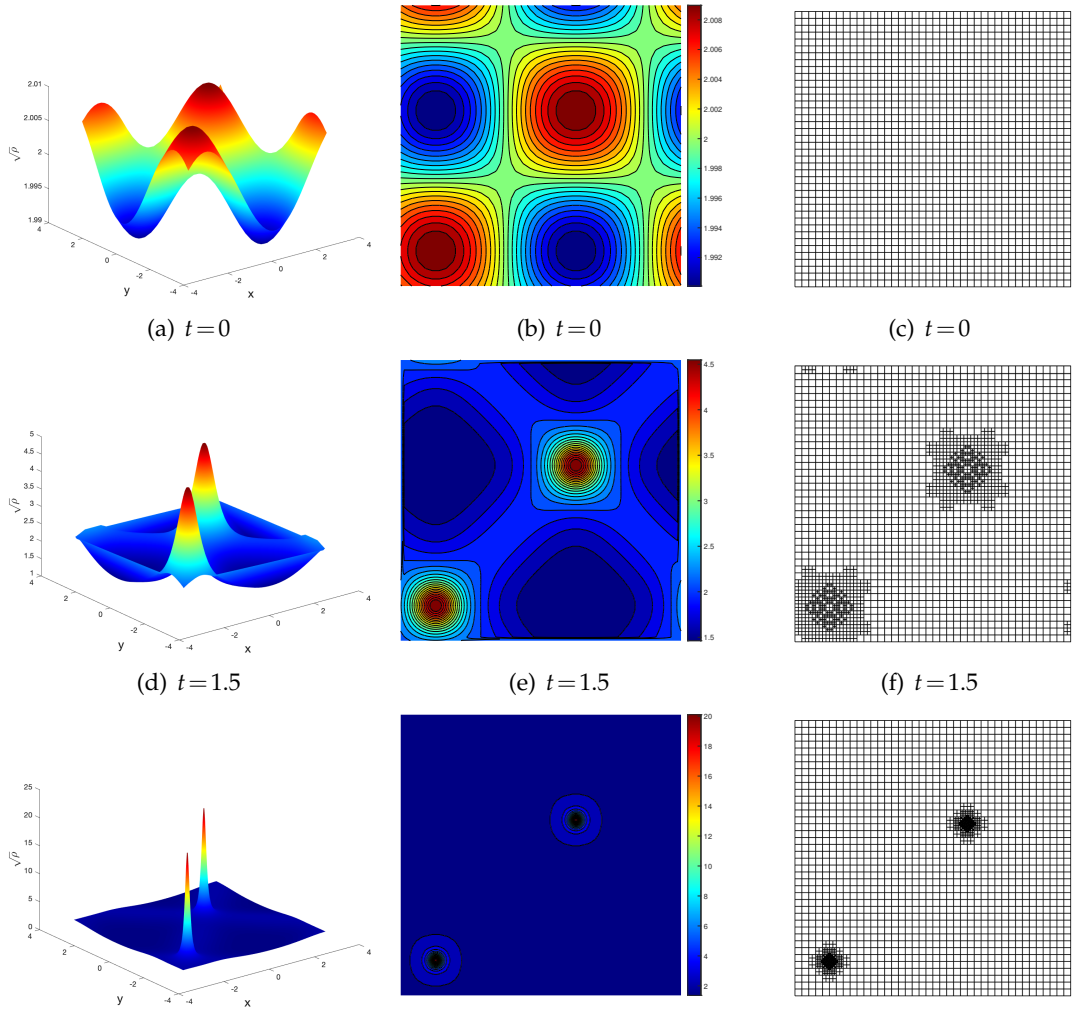

(a) $t=0$ (b) $t=0$ (c) $t=0$

(d) $t=1.5$ (e) $t=1.5$ (f) $t=1.5$

(g) $t=1.5813$ (h) $t=1.5813$ (i) $t=1.5813$

Figure 6: Example 6.6. Blow up phenomenon for 2D QHD equations with initial density (6.7) computed with the IEK-C scheme. The square root of the density and corresponding adaptive mesh. Q^2 elements and initial mesh of 40×40 cells.

7 Concluding remarks

In this paper, we have developed an energy conservative LDG discretization for the general EK-equations with a variable capillarity coefficient, namely the GEK-C scheme. The GEK-C scheme achieves optimal order of accuracy when alternating numerical fluxes are used, but loses one order of accuracy for central numerical fluxes when odd degree polynomial basis functions are adopted. The QHD equations, as a special case of the EK-

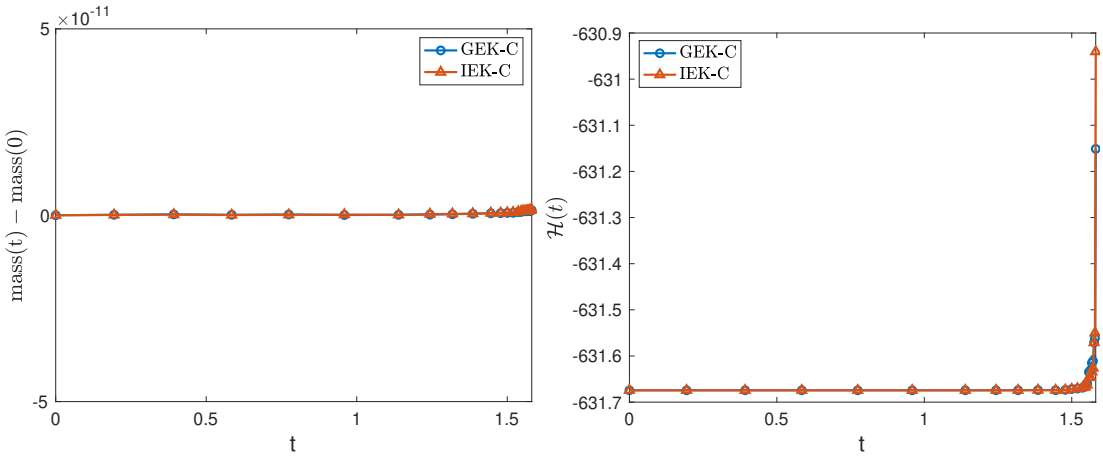

(a) Mass loss evolution (b) Energy evolution

Figure 7: Example 6.6. Blow up phenomenon for 2D QHD equations with initial density (6.7) computed with the IEK-C scheme. Mass loss and energy evolution. Q^2 elements and initial mesh of 40×40 cells.

equations with an irrotational velocity field, have been widely used in quantum physics. As a consequence, we specially designed a relatively simple LDG discretization, namely the IEK-C scheme, for the EK-equations with an irrotational velocity field, which is well suited to solving the QHD equations with high order accuracy. The energy conservation property of the GEK-C and IEK-C schemes was proven for the semi-discrete sense. When coupled with semi-implicit SDC methods, the high-order accuracy and capability of the proposed methods were demonstrated in various numerical experiments.

A challenging direction for future work would be to extend the theoretical proof of energy conservation property from the semi-discrete LDG discretizations to the fully discrete schemes when coupled with semi-implicit SDC methods. Also, the KKT limiter proposed in [48, 56, 57] opens avenues for developing time-implicit high order accurate positivity-preserving discretizations for the EK-equations.

Appendix A. Derivation of LDG term in Eq. (3.3b)

In this appendix, we provide the details of the derivation of the last term in Eq. (3.3b).

Multiplying $\rho_h\nabla(f_h-r_h+s_h+\frac{1}{2}|\mathbf{u}_h|^2)$ with the test function $\boldsymbol{\psi}$, integrating over element $K\in\mathcal{T}_h$ and performing integration by parts, we obtain

$$-\int_K\left(f_h-r_h+s_h+\frac{1}{2}|\mathbf{u}_h|^2\right)\nabla\cdot(\rho_h\boldsymbol{\psi})d\mathbf{x}+\int_{\partial K}\rho_h^-\left(\widehat{f_h}-\widehat{r_h}+\widehat{s_h}+\frac{1}{2}\widehat{|\mathbf{u}_h|^2}\right)\boldsymbol{\psi}^-\cdot\mathbf{n}_K ds.$$

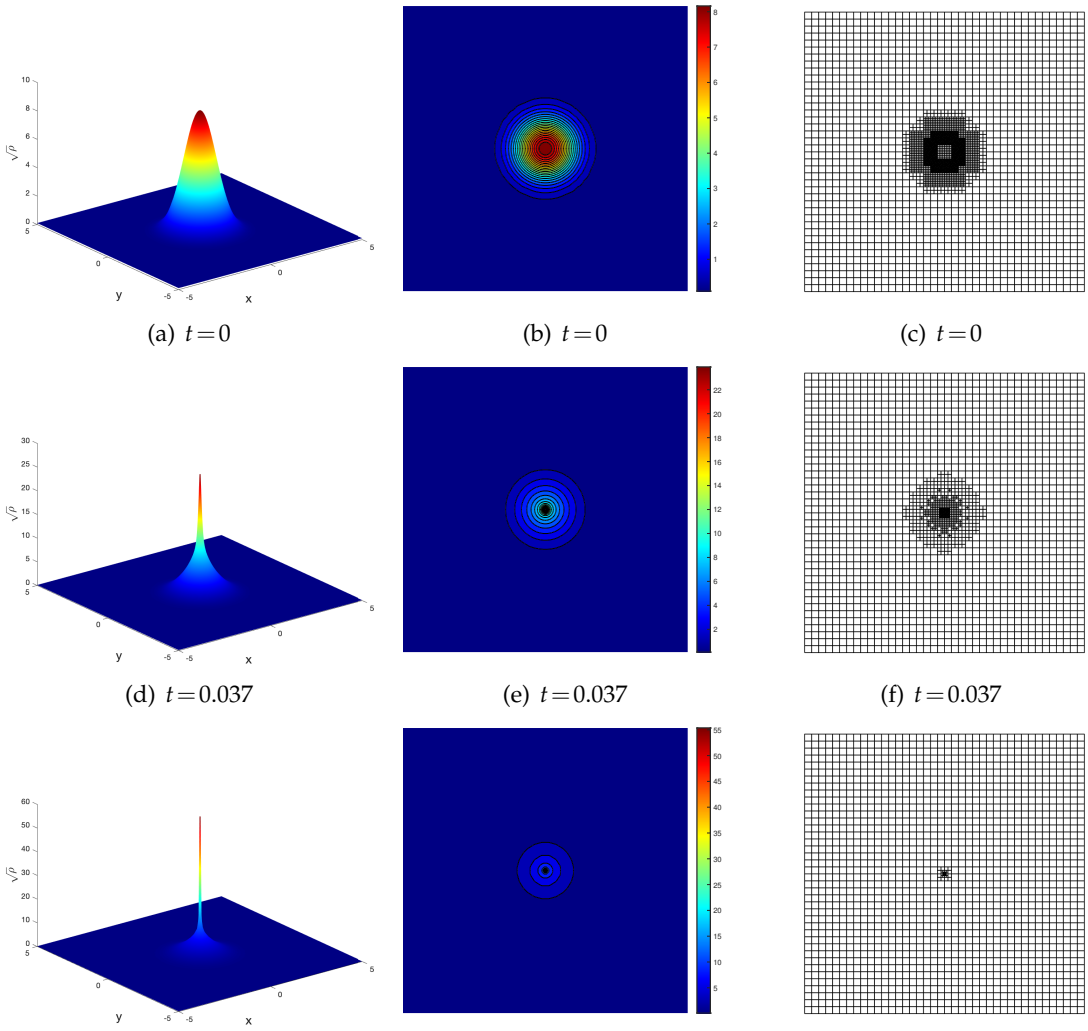

(a) $t=0$ (b) $t=0$ (c) $t=0$

(d) $t=0.037$ (e) $t=0.037$ (f) $t=0.037$

(g) $t=0.0396$ (h) $t=0.0396$ (i) $t=0.0396$

Figure 8: Example 6.6. Blow up phenomenon for 2D QHD equations with initial density (6.8) computed with the IEK-C scheme. The square root of the density and corresponding adaptive mesh. P^3 elements and initial mesh of 40×40 cells.

Integrating by parts once again yields

$$\int_K \rho_h \nabla\left(f_h - r_h + s_h + \frac{1}{2}|\mathbf{u}_h|^2\right)\cdot\boldsymbol{\psi}\, d\mathbf{x}$$
$$-\int_{\partial K}\rho_h^-\left(\left(f_h^- - r_h^- + s_h^- + \frac{1}{2}|\mathbf{u}_h^-|^2\right) - \left(\widehat{f_h} - \widehat{r_h} + \widehat{s_h} + \frac{1}{2}\widehat{|\mathbf{u}_h|^2}\right)\right)\boldsymbol{\psi}^-\cdot\mathbf{n}_K\, ds.$$

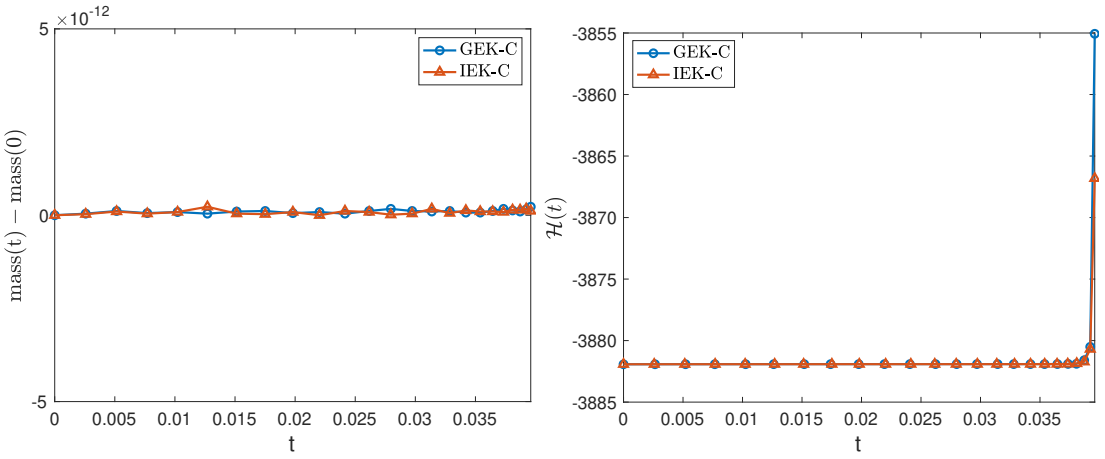

(a) Mass loss evolution (b) Energy evolution

Figure 9: Example 6.6. Blow up phenomenon for 2D QHD equations with initial density (6.8) computed with the IEK-C scheme. Mass loss and energy evolution. P^3 elements and initial mesh of 40×40 cells.

After summation over all elements in the tessellation $\mathcal{T}_h$, we have

$$\begin{aligned}
&\sum_{K\in\mathcal{T}_h}\int_K \rho_h\nabla\Big(f_h-r_h+s_h+\frac{1}{2}|\mathbf{u}_h|^2\Big)\cdot\boldsymbol{\psi}\,d\mathbf{x}\\
&\quad-\sum_{e\in\Gamma_I}\int_e\Big(\rho_h^L\Big(\Big(f_h^L-r_h^L+s_h^L+\frac{1}{2}|\mathbf{u}_h^L|^2\Big)-\Big(\widehat{f_h}-\widehat{r_h}+\widehat{s_h}+\frac{1}{2}\widehat{|\mathbf{u}_h|^2}\Big)\Big)\boldsymbol{\psi}^L\cdot\mathbf{n}_L\\
&\quad+\rho_h^R\Big(\Big(f_h^R-r_h^R+s_h^R+\frac{1}{2}|\mathbf{u}_h^R|^2\Big)-\Big(\widehat{f_h}-\widehat{r_h}+\widehat{s_h}+\frac{1}{2}\widehat{|\mathbf{u}_h|^2}\Big)\Big)\boldsymbol{\psi}^R\cdot\mathbf{n}_R\Big)\,ds. \qquad (A.1)
\end{aligned}$$

If we choose

$$\begin{aligned}
&\widehat{f_h}=\{f_h\}-\alpha_1[\![f_h]\!],\quad \widehat{r_h}=\{r_h\}-\alpha_1[\![r_h]\!],\\
&\widehat{s_h}=\{s_h\}-\alpha_1[\![s_h]\!],\quad \widehat{|\mathbf{u}_h|^2}=\{|\mathbf{u}_h|^2\}-\alpha_1[\![|\mathbf{u}_h|^2]\!],
\end{aligned}$$

then

$$\begin{aligned}
&f_h^L-\widehat{f_h}=\Big(\frac{1}{2}-\alpha_1\Big)f_h^L+\Big(-\frac{1}{2}+\alpha_1\Big)f_h^R,\qquad f_h^R-\widehat{f_h}=\Big(-\frac{1}{2}-\alpha_1\Big)f_h^L+\Big(\frac{1}{2}+\alpha_1\Big)f_h^R,\\
&r_h^L-\widehat{r_h}=\Big(\frac{1}{2}-\alpha_1\Big)r_h^L+\Big(-\frac{1}{2}+\alpha_1\Big)r_h^R,\qquad r_h^R-\widehat{r_h}=\Big(-\frac{1}{2}-\alpha_1\Big)r_h^L+\Big(\frac{1}{2}+\alpha_1\Big)r_h^R,\\
&s_h^L-\widehat{s_h}=\Big(\frac{1}{2}-\alpha_1\Big)s_h^L+\Big(-\frac{1}{2}+\alpha_1\Big)s_h^R,\qquad s_h^R-\widehat{s_h}=\Big(-\frac{1}{2}-\alpha_1\Big)s_h^L+\Big(\frac{1}{2}+\alpha_1\Big)s_h^R,\\
&|\mathbf{u}_h^L|^2-\widehat{|\mathbf{u}_h|^2}=\Big(\frac{1}{2}-\alpha_1\Big)|\mathbf{u}_h^L|^2+\Big(-\frac{1}{2}+\alpha_1\Big)|\mathbf{u}_h^R|^2,\\
&|\mathbf{u}_h^R|^2-\widehat{|\mathbf{u}_h|^2}=\Big(-\frac{1}{2}-\alpha_1\Big)|\mathbf{u}_h^L|^2+\Big(\frac{1}{2}+\alpha_1\Big)|\mathbf{u}_h^R|^2.
\end{aligned}$$

Using these relations (A.1) transforms into

$$\sum_{K\in\mathcal{T}_h}\int_K \rho_h \nabla\Big(f_h - r_h + s_h + \frac{1}{2}|\mathbf{u}_h|^2\Big)\cdot\boldsymbol{\psi}\,d\mathbf{x} - \sum_{e\in\Gamma_I}\int_e \bigg(\Big(\frac{1}{2}-\alpha_1\Big)\rho_h^L\boldsymbol{\psi}^L + \Big(\frac{1}{2}+\alpha_1\Big)\rho_h^R\boldsymbol{\psi}^R\bigg)$$
$$\cdot\bigg(\Big(f_h^L - r_h^L + s_h^L + \frac{1}{2}|\mathbf{u}_h^L|^2\Big)\mathbf{n}_L + \Big(f_h^R - r_h^R + s_h^R + \frac{1}{2}|\mathbf{u}_h^R|^2\Big)\mathbf{n}_R\bigg)\,ds,$$

which can be written as

$$\sum_{K\in\mathcal{T}_h}\int_K \rho_h\boldsymbol{\psi}\cdot\nabla\Big(f_h - r_h + s_h + \frac{1}{2}|\mathbf{u}_h|^2\Big)\,d\mathbf{x}$$
$$-\sum_{e\in\Gamma_I}\int_e (\{\rho_h\boldsymbol{\psi}\} + \alpha_1[\![\rho_h\boldsymbol{\psi}]\!])\cdot\Big[f_h - r_h + s_h + \frac{1}{2}|\mathbf{u}_h|^2\Big]\,ds,$$

and is exactly the term

$$-\widetilde{\mathcal{D}}^2\Big(\rho_h\boldsymbol{\psi}, f_h - r_h + s_h + \frac{1}{2}|\mathbf{u}_h|^2; \alpha_1\Big)$$

in (3.3b).

Acknowledgements

X. Meng would like to acknowledge the China Scholarship Council (CSC) grant No. 201806340215 for giving the opportunity and financial support to study at the University of Twente in the Netherlands. The research of Yan Xu is supported by NSFC grant No. 12071455. The research of J. J. W. van der Vegt was partially supported by the University of Science and Technology of China (USTC), Hefei, Anhui, China.

References

[1] P. ANTONELLI AND P. MARCATI, *On the finite energy weak solutions to a system in quantum fluid dynamics*, Commun. Math. Phys., 287(2) (2009), pp. 657–686.
[2] P. ANTONELLI AND S. SPIRITO, *Global existence of weak solutions to the Navier-Stokes-Korteweg equations*, Annales de l'Institut Henri Poincaré C, 39(1) (2022), pp. 171–200.
[3] C. AUDIARD, *On the time of existence of solutions of the Euler-Korteweg system*, Annales de la Faculté des Sciences de Toulouse: Mathématiques, 30(5) (2021), pp. 1139–1183.
[4] C. AUDIARD AND B. HASPOT, *Global well-posedness of the Euler–Korteweg system for small irrotational data*, Commun. Math. Phys., 351(1) (2017), pp. 201–247.
[5] S. BENZONI-GAVAGE, Propagating Phase Boundaries and Capillary Fluids, PhD thesis, CIRM-Fondazione Bruno Kessler, 2010.
[6] S. BENZONI-GAVAGE, R. DANCHIN, AND S. DESCOMBES, *Well-posedness of one-dimensional Korteweg models*, Electronic J. Differential Equations, 59 (2006), pp. 1–35.
[7] S. BENZONI-GAVAGE, R. DANCHIN, AND S. DESCOMBES, *On the well-posedness for the Euler-Korteweg model in several space dimensions*, Indiana University Mathematics J., 56(4) (2007), pp. 1499–1579.

[8] S. BENZONI-GAVAGE, L. MAZET, S. DESCOMBES, AND D. JAMET, *Structure of Korteweg models and stability of diffuse interfaces*, Interfaces and Free Boundaries, 7(4) (2005), pp. 371–414.
[9] M. BRAACK AND A. PROHL, *Stable discretization of a diffuse interface model for liquid-vapor flows with surface tension*, ESAIM: Mathematical Modelling and Numerical Analysis, 47(2) (2013), pp. 401–420.
[10] D. BRESCH, F. COUDERC, P. NOBLE, AND J.-P. VILA, *A generalization of the quantum Bohm identity: Hyperbolic CFL condition for Euler–Korteweg equations*, Comptes Rendus Mathematique, 354(1) (2016), pp. 39–43.
[11] D. BRESCH, M. GISCLON, AND I. LACROIX-VIOLET, *On Navier–Stokes–Korteweg and Euler–Korteweg systems: application to quantum fluids models*, Arch. Rational Mech. Anal., 233(3) (2019), pp. 975–1025.
[12] R. CARLES, R. DANCHIN, AND J.-C. SAUT, *Madelung, Gross–Pitaevskii and Korteweg*, Nonlinearity, 25(10) (2012), 2843.
[13] A. CHERTOCK, P. DEGOND, AND J. NEUSSER, *An asymptotic-preserving method for a relaxation of the Navier-Stokes-Korteweg equations*, J. Comput. Phys., 335 (2017), pp. 387–403.
[14] B. COCKBURN AND C.-W. SHU, *The local discontinuous Galerkin method for time-dependent convection-diffusion systems*, SIAM J. Numer. Anal., 35(6) (1998), pp. 2440–2463.
[15] F. DHAOUADI, An Augmented Lagrangian Approach for Euler-Korteweg Type Equations, PhD thesis, Université Paul Sabatier-Toulouse III, 2020.
[16] F. DHAOUADI AND M. DUMBSER, *A first order hyperbolic reformulation of the Navier-Stokes-Korteweg system based on the GPR model and an augmented Lagrangian approach*, J. Comput. Phys., 470 (2022), 111544.
[17] F. DHAOUADI, N. FAVRIE, AND S. GAVRILYUK, *Extended Lagrangian approach for the defocusing nonlinear Schrödinger equation*, Studies Appl. Math., 142(3) (2019), pp. 336–358.
[18] F. DHAOUADI, S. GAVRILYUK, AND J.-P. VILA, *Hyperbolic relaxation models for thin films down an inclined plane*, Appl. Math. Comput., 433 (2022), 127378.
[19] D. DIEHL, J. KREMSER, D. KRÖNER, AND C. ROHDE, *Numerical solution of Navier–Stokes–Korteweg systems by local discontinuous Galerkin methods in multiple space dimensions*, Appl. Math. Comput., 272 (2016), pp. 309–335.
[20] J. E. DUNN AND J. SERRIN, *On the thermomechanics of interstitial working*, In The Breadth and Depth of Continuum Mechanics, pages 705–743. Springer, 1986.
[21] X. FENG, T. TANG, AND J. YANG, *Long time numerical simulations for phase-field problems using p-adaptive spectral deferred correction methods*, SIAM J. Sci. Comput., 37(1) (2015), pp. A271–A294.
[22] D. FERRY AND J.-R. ZHOU, *Form of the quantum potential for use in hydrodynamic equations for semiconductor device modeling*, Phys. Rev. B, 48(11) (1993), 7944.
[23] J. GIESSELMANN, C. LATTANZIO, AND A. E. TZAVARAS, *Relative energy for the Korteweg theory and related Hamiltonian flows in gas dynamics*, Arch. Rational Mech. Anal., 223(3) (2017), pp. 1427–1484.
[24] J. GIESSELMANN, C. MAKRIDAKIS, AND T. PRYER, *Energy consistent discontinuous Galerkin methods for the Navier–Stokes–Korteweg system*, Math. Comput., 83(289) (2014), pp. 2071–2099.
[25] H. GOMEZ, T. J. HUGHES, X. NOGUEIRA, AND V. M. CALO, *Isogeometric analysis of the isothermal Navier-Stokes-Korteweg equations*, Comput. Methods Appl. Mech. Eng., 199(25-28) (2010), pp. 1828–1840.
[26] J. GRANT, *Pressure and stress tensor expressions in the fluid mechanical formulation of the Bose condensate equations*, J. Phys. A: Math. Nuclear General, 6(11) (1973), L151.
[27] D. GRECU, R. FEDELE, S. DE NICOLA, A. GRECU, AND A. VISINESCU, *Periodic and solitary*

wave solutions of generalized nonlinear Schrodinger equation using a Madelung fluid description, Romanian J. Phys., 55(9-10) (2010), pp. 980–994.

[28] R. GUO, Y. XIA, AND Y. XU, *Semi-implicit spectral deferred correction methods for highly nonlinear partial differential equations*, J. Comput. Phys., 338 (2017), pp. 269–284.

[29] R. GUO AND Y. XU, *Local discontinuous Galerkin method and high order semi-implicit scheme for the phase field crystal equation*, SIAM J. Sci. Comput., 38(1) (2016), pp. A105–A127.

[30] T. HITZ, J. KEIM, C.-D. MUNZ, AND C. ROHDE, *A parabolic relaxation model for the Navier-Stokes-Korteweg equations*, J. Comput. Phys., 421 (2020), 109714.

[31] M. HOEFER, M. ABLOWITZ, I. CODDINGTON, E. A. CORNELL, P. ENGELS, AND V. SCHWEIKHARD, *Dispersive and classical shock waves in Bose-Einstein condensates and gas dynamics*, Phys. Rev. A, 74(2) (2006), 023623.

[32] C. G. J. JACOBI, Fundamenta Nova Theoriae Functionum Ellipticarum, Cambridge University Press, 2013.

[33] J. KEIM, C.-D. MUNZ, AND C. ROHDE, *A relaxation model for the non-isothermal Navier-Stokes-Korteweg equations in confined domains*, J. Comput. Phys., 474 (2023), 111830.

[34] D. J. KORTEWEG, *Sur la forme que prennent les équations du mouvements des fluides si l'on tient compte des forces capillaires causées par des variations de densité considérables mais connues et sur la théorie de la capillarité dans l'hypothèse d'une variation continue de la densité*, Archives Néerlandaises des Sciences Exactes et Naturelles, 6 (1901), pp. 1–24.

[35] J. LIU, H. GOMEZ, J. A. EVANS, T. J. HUGHES, AND C. M. LANDIS, *Functional entropy variables: a new methodology for deriving thermodynamically consistent algorithms for complex fluids, with particular reference to the isothermal Navier–Stokes–Korteweg equations*, J. Comput. Phys., 248 (2013), pp. 47–86.

[36] J. LIU, J. QIU, O. HU, N. ZHAO, M. GOMAN, AND X. LI, *Adaptive Runge–Kutta discontinuous Galerkin method for complex geometry problems on Cartesian grid*, Int. J. Numer. Methods Fluids, 73(10) (2013), pp. 847–868.

[37] M. LOFFREDO AND L. MORATO, *On the creation of quantized vortex lines in rotating He II*, Il Nuovo Cimento B (1971-1996), 108(2) (1993), pp. 205–215.

[38] E. MADELUNG, *Quantentheorie in hydrodynamischer form*, Zeitschrift für Physik, 40(3) (1927), pp. 322–326.

[39] X. MENG AND Y. XU, *Adaptive local discontinuous Galerkin methods with semi-implicit time discretizations for the Navier-Stokes equations*, Adv. Aerodyn., 4(1) (2022), pp. 1–31.

[40] M. L. MINION, *Semi-implicit spectral deferred correction methods for ordinary differential equations*, Commun. Math. Sci., 1(3) (2003), pp. 471–500.

[41] J. NEUSSER, C. ROHDE, AND V. SCHLEPER, *Relaxation of the Navier-Stokes-Korteweg equations for compressible two-phase flow with phase transition*, Int. J. Numer. Methods Fluids, 79(12) (2015), pp. 615–639.

[42] P. NOBLE AND J.-P. VILA, *Stability theory for difference approximations of Euler–Korteweg equations and application to thin film flows*, SIAM J. Numer. Anal., 52(6) (2014), pp. 2770–2791.

[43] A. PECENKO, J. KUERTEN, AND C. VAN DER GELD, *A diffuse-interface approach to two-phase isothermal flow of a Van der Waals fluid near the critical point*, Int. J. Multiphase Flow, 36(7) (2010), pp. 558–569.

[44] A. PECENKO, L. VAN DEURZEN, J. G. KUERTEN, AND C. VAN DER GELD, *Non-isothermal two-phase flow with a diffuse-interface model*, Int. J. Multiphase Flow, 37(2) (2011), pp. 149–165.

[45] Z. TAO, J. HUANG, Y. LIU, W. GUO, AND Y. CHENG, *An adaptive multiresolution ultra-weak discontinuous Galerkin method for nonlinear Schrödinger equations*, Commun. Appl. Math. Comput., 4(1) (2022), pp. 60–83.

[46] L. TIAN, Y. XU, J. KUERTEN, AND J. J. VAN DER VEGT, *A local discontinuous Galerkin method for the (non)-isothermal Navier–Stokes–Korteweg equations*, J. Comput. Phys., 295 (2015), pp. 685–714.
[47] L. TIAN, Y. XU, J. G. KUERTEN, AND J. J. VAN DER VEGT, *An h-adaptive local discontinuous Galerkin method for the Navier–Stokes–Korteweg equations*, J. Comput. Phys., 319 (2016), pp. 242–265.
[48] J. J. W. VAN DER VEGT, Y. XIA, AND Y. XU, *Positivity preserving limiters for time-implicit higher order accurate discontinuous Galerkin discretizations*, SIAM J. Sci. Comput., 41(3) (2019), pp. A2037–A2063.
[49] J. D. VAN DER WAALS, *The thermodynamic theory of capillarity under the hypothesis of a continuous variation of density*, J. Stat. Phys., 20(2) (1979), pp. 200–244.
[50] R. E. WYATT, Quantum Dynamics with Trajectories: Introduction to Quantum Hydrodynamics, Volume 28. Springer Science & Business Media, 2005.
[51] Y. XIA, *A fully discrete stable discontinuous Galerkin method for the thin film epitaxy problem without slope selection*, J. Comput. Phys., 280 (2015), pp. 248–260.
[52] Y. XU AND C.-W. SHU, *Local discontinuous Galerkin methods for nonlinear Schrödinger equations*, J. Comput. Phys., 205(1) (2005), pp. 72–97.
[53] Y. XU AND C.-W. SHU, *A local discontinuous Galerkin method for the Camassa–Holm equation*, SIAM J. Numer. Anal., 46(4) (2008), pp. 1998–2021.
[54] Y. XU AND C.-W. SHU, *Local discontinuous Galerkin methods for high-order time-dependent partial differential equations*, Commun. Comput. Phys., 7(1) (2010), pp. 1–46.
[55] Y. XU AND C.-W. SHU, *Local discontinuous Galerkin methods for the Degasperis-Procesi equation*, Commun. Comput. Phys., 10(2) (2011), pp. 474–508.
[56] F. YAN, J. J. W. VAN DER VEGT, Y. XIA, AND Y. XU, *Higher order accurate bounds preserving time-implicit discretizations for the chemically reactive Euler equations*. Commun. Comput. Phys., to appear.
[57] F. YAN, J. J. W. VAN DER VEGT, Y. XIA, AND Y. XU, *Entropy dissipative higher order accurate positivity preserving time-implicit discretizations for nonlinear degenerate parabolic equations*, J. Comput. Appl. Math., 441 (2024), 115674.
[58] J. YAN AND C.-W. SHU, *A local discontinuous Galerkin method for KdV type equations*, SIAM J. Numer. Anal., 40(2) (2002), pp. 769–791.
[59] R. ZHANG, X. YU, M. LI, AND X. LI, *A conservative local discontinuous Galerkin method for the solution of nonlinear Schrödinger equation in two dimensions*, Science China Mathematics, 60(12) (2017), pp. 2515–2530.
[60] R.-P. ZHANG, *Compact implicit integration factor methods for some complex-valued nonlinear equations*, Chinese Phys. B, 21(4) (2012), 040205.
[61] J. ZHAO, Q. ZHANG, Y. YANG, AND Y. XIA, *Conservative discontinuous Galerkin methods for the nonlinear Serre equations*, J. Comput. Phys., 421 (2020), 109729.